ADVANCED ENERGY MATERIALS
www.advenergymat.de

Structural Design of Cathodes for Li-S Batteries

Michael A. Pope and Ilhan A. Aksay**

Battery technologies involving Li-S chemistries have been touted as one of the most promising next generation systems. The theoretical capacity of sulfur is nearly an order of magnitude higher than current Li-ion battery insertion cathodes and when coupled with a Li metal anode, Li-S batteries promise specific energies nearly five-fold higher. However, this assertion only holds if sulfur cathodes could be designed in the same manner as cathodes for Li-ion batteries. Here, the recent efforts to engineer high capacity, thick, sulfur-based cathodes are explored. Various works are compared in terms of capacity, areal mass loading, and fraction of conductive additive, which are the critical parameters dictating the potential for a device to achieve a specific energy higher than current Li-ion batteries (i.e., >200 Wh kg^{-1}). While an inferior specific energy is projected in the majority of cases, several promising strategies have the potential to achieve >500 Wh kg^{-1}. The challenges associated with the limited cycle-life of these systems due to both the polysulfide shuttle phenomenon and the rapid degradation of the Li metal anode that is experienced at the current densities required to charge high specific energy batteries in a reasonable timeframe are also discussed.

1. Introduction

Advancements in Li-ion batteries over the last 25 years have led to high hopes of wide-spread vehicle electrification and grid-level energy storage that will make global energy generation and usage more efficient, less dependent on fossil fuels and lead to reduced emissions of greenhouse gases.[1–4] While Li-ion batteries have proven sufficient to power fully electric cars as exemplified by companies such as Tesla, Toyota, and BMW, widespread use of electric vehicles will require significant improvements in the energy storage technologies they use.[5]

Prof. M. A. Pope
Department of Chemical Engineering
Waterloo Institute for Nanotechnology
University of Waterloo
Waterloo, ON N2L 3G1, Canada
E-mail: michael.pope@uwaterloo.ca
Prof. M. A. Pope
Vorbeck Princeton Research Center
Vorbeck Materials Corp.
Monmouth Junction, NJ 08852, USA
Prof. I. A. Aksay
Department of Chemical and Biological Engineering
Princeton University
Princeton, NJ 08544, USA
E-mail: iaksay@princeton.edu

DOI: 10.1002/aenm.201500124

Optimized Li-ion batteries can now achieve specific energies (E) up to ≈200 Wh kg^{-1} but only marginal improvements to this technology are expected in the near future as cells reach their theoretical limits.[3,5,6] While significant progress has been made,[7] continued improvements to drive range, decreased charging times and more efficient operation at high power are required to effectively accept energy generated during braking[8] and to make charging times more convenient for consumers who are used to spending only a few minutes filling their tanks with gas as opposed to overnight charging required by current battery systems.

Cost is also a factor. Most Li-ion batteries are too expensive to be economical for grid level storage and also make the price of electric vehicles prohibitively expensive for the average consumer. A state-of-the-art Li-ion battery pack costs ≈$400 per kWh,[7] a figure which needs to be reduced to ≈$150 per kWh as suggested by the US Advanced Battery Consortium.[8] In a recent review, Larcher and Tarascon also pointed out the importance of the sustainability of materials and processes used to make these batteries.[5] In order to reduce the energy and fossil fuel consumption associated with materials extraction and battery manufacturing we must look towards abundant, accessible, recyclable materials and low temperature production processes.[5]

1.1. Advantages of Li-S Batteries

Lithium-sulfur (Li-S) batteries are regarded as one of the most promising systems as they hold the potential to address most of the challenges discussed above. Sulfur is abundant and inexpensive, currently produced in large quantities, as a waste product of the oil and gas industry and is also naturally occurring, being the 16th most abundant element in the Earth's lithosphere.[9] Sulfur's low melting point (115.2 °C) and sublimation temperature lead to potentially more energy efficient manufacturing approaches. Most importantly, the electrochemical reduction of sulfur: $S + 2Li^+ \rightarrow Li_2S + 2e^-$, yields a theoretical capacity of 1672 mAh g^{-1} sulfur which is an order of magnitude larger than state-of-the-art Li-ion cathode materials such as $LiCoO_2$, $LiFePO_4$, and NCA which exhibit theoretical capacities of 140-180 mAh g^{-1}.[1,3,5] This high cathode capacity (Q_C) arises through a combination of sulfur's low molecular weight (M_W = 32.06) and the net two-electrons (n = 2) generated through the

various conversion reactions which occur in the electrochemical cell (since $Q_C = nF/3.6M_W$). When coupled with a high capacity Li metal anode (Q_A = 3860 mAh g^{-1}), the cell exhibits a potential of $U \approx 2.2$ V and a combined capacity of $Q^* = 1167$ mAh g^{-1} which results in a specific energy of $E^* = Q \cdot U = 2567$ Wh kg^{-1}. Both Q^* and E^* are specific to the mass of anode and cathode active materials only. Due to the required additional mass of other cell components, practical specific energies (E) of only ≈350 Wh kg^{-1} have been reported at the prototype level.[10] As will be discussed later, recent advancements and optimized cell design have the potential to boost E to the 500–600 Wh kg^{-1} range. On the other hand, the low density of sulfur and Li metal compared to traditional metal oxides offsets any gains in energy density (i.e., energy per unit volume typically expressed in Wh L^{-1}).[6] For example, replacing Li-ion batteries in an electric vehicle with a Li-S system of equal energy storage capacity will significantly reduce the weight of the vehicle (thus improving its efficiency and range) but is expected to take up a similar volume within the vehicle.

1.2. Current Challenges of Li-S Batteries

While the Li-S system will potentially impact applications which would benefit from significant weight reduction, there are several challenges that must be addressed that impact the overall cell design, the cycle-life, safety and reliability compared to Li-ion cells. Sulfur and the final discharge product Li_2S are electrically insulating.[9] Sulfur is also not a Li ion conductor. For an electrochemical reaction to occur there must be a concurrent transfer of both electrons and ions. Such a situation cannot be achieved at practical rates for thick sulfur films. For this reason, sulfur electrodes are typically mixed with a high surface area conducting material to minimize the effective sulfur thickness between the conductor and the electrolyte to facilitate electronic and ionic transport.[11] Many strategies have been developed to disperse sulfur in a variety of conducting materials including high surface area carbonaceous materials,[12–36] polymers,[37–40] metals,[41–43] metal oxides, [44–49] and metal organic frameworks.[50,51] The goal of these strategies is to maximize the amount of sulfur which can be accessed electrochemically at reasonable current densities while minimizing the mass and volume of the conductive phase necessary (as this adds to the mass of inactive material in the battery) which can constitute a major fraction of the cathode mass and volume (often > 50%).

As illustrated in **Figure 1**, Li-ion batteries operate by reversible intercalation and de-intercalation reactions at both the anode and cathode and rely only on the transport of Li ions between these insertion compounds (typically a graphite anode[52] and a transition metal oxide cathode[53]). On the other hand, a Li-S battery involves a conversion reaction where various intermediate species referred to as polysulfides are produced.[54] In particular the Li_2S_n ($3 \le n \le 6$), generated during the conversion reaction are soluble in most commonly used organic electrolytes.[55] This solubility enables the transport of sulfur species to the Li metal anode where they can react to form the insoluble Li_2S, reducing the Coulombic efficiency and the reversible capacity of the cell.[56] On the other hand, this solubility provides a mechanism for the redistribution of sulfur onto the conductive support material during cycling if the sulfur was not dispersed homogeneously to begin with.[36]

Furthermore, it is known that cathodes based on elemental sulfur are not compatible with traditional carbonate-based electrolytes.[57,58] Polysulfide intermediates react rapidly and irreversibly with the carbonate solvent,[57] thereby exhibiting a high initial capacity which drops to nearly zero on the second cycle. This chemical instability has led to the use of the alternative and inert ether-based electrolytes typically comprised of a mixture of dioxolane (DOX) and dimethyl ether (DME).[59] Unfortunately this solvent system poses several challenges associated with its high vapor pressure such as its reduced flashpoint which bring about safety concerns and practical challenges involving solvent boiling during vacuum processing.

In addition to the polysulfide problem, the Li metal anode required to achieve high specific energy is unstable with cycling. Unlike insertion anodes such as graphite which change in volume by ≈20% during cycling, lithium is completely removed from the metal during discharge and replenished upon charge

Michael Pope completed his B. Eng. at McMaster University and his Ph.D. at Princeton University in Chemical Engineering. After graduating, he carried out research and development on graphene-based technologies at Vorbeck Materials Corp. including acting as technical lead on a developmental program to commercialize graphene-based Li-S batteries. Michael is now an Assistant Professor in the Department of Chemical Engineering at the University of Waterloo where his research is focused on advanced materials and devices for improved energy storage, generation and sensing technologies.

Ilhan Aksay is a Professor in the Department of Chemical and Biological Engineering of Princeton University. He earned his Ph.D. (1973) in materials science and engineering at the University of California, Berkeley. His research interests emphasize the utilization of self-assembly techniques in materials processing. His most recent work on functionalized graphene demonstrated many advantages in technologies ranging from nanocomposites to electrochemical devices for chemical sensing, energy harvesting, and energy storage.

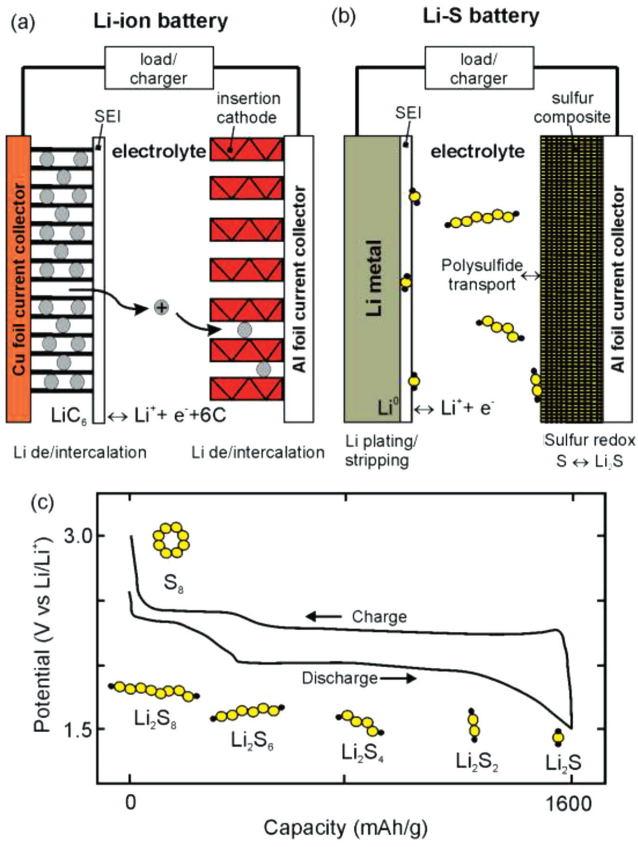

Figure 1. Overview of Li-S batteries compared to Li-ion batteries. a) Schematic of a typical Li-ion battery comprised of a lithiated graphite (LiC_6) anode and an insertion cathode such as $LiCoO_2$ or $LiFePO_4$. On discharge, LiC_6 is oxidized, sending an electron through the circuit while Li ions de-intercalate and are inserted into the cathode which is reduced in the process. The reverse occurs when the battery is charged. b) Schematic of a Li-S battery comprised of a Li metal anode and a sulfur composite cathode. Li metal is oxidized producing electrons and liberating Li ions. The sulfur cathode is reduced and forms various polysulfide intermediates. Some of the polysulfides are soluble in the electrolyte and are shown to diffuse/migrate to the anode. c) Typical charge/discharge profile of a Li-S battery indicating the regions where various polysulfides are produced or consumed.

leading to effectively infinite volume change. The reaction products formed between Li metal and the electrolyte form the solid electrolyte interface (SEI),[60] a passivation layer which inhibits further reaction between Li metal and the electrolyte. However, the large volume change typically causes cracks and fissures to open in the SEI layer upon each charge/discharge cycle which consumes both electrolyte and dissolved polysulfides.[61] This also causes the inhomogeneous deposition of Li metal during charge leading to dendritic growth and the development of porous (i.e., mossy) Li metal structures.[61] The main failure mechanism is thought to be related to the formation of porous Li metal with cycling.[62,63] The extensive amount of SEI required to passivate this high surface area leads to both sulfur depletion and electrolyte starvation causing capacity loss and eventual cell failure. As will be discussed further, this is one of the most challenging aspects facing the successful development of Li-S batteries.

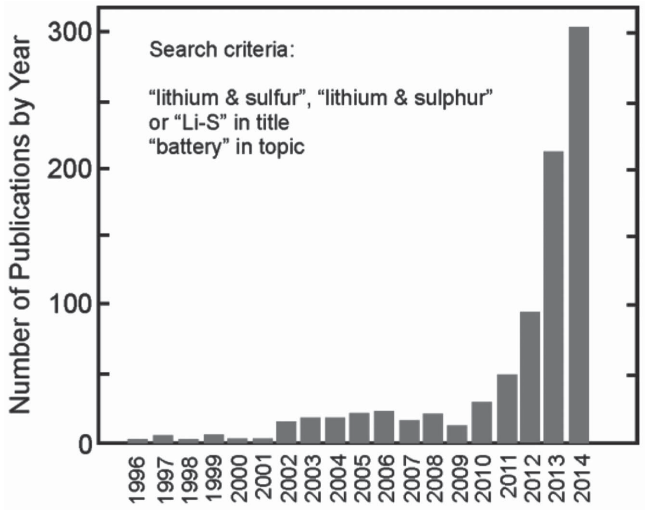

Figure 2. Approximate number of publications in the Li-S battery field as a function of year. Citation report for "lithium & sulfur" or "lithium & sulphur" or "Li-S" in the publication title. Retrieved from ISI Web of Knowledge on December 16, 2014.

1.3. Scope of this Review

Over just the last handful of years, there has been a resurgence of research on Li-S batteries exploding with efforts to tackle the challenges discussed above with over 300 publications in 2014 alone. (**Figure 2**) As it is nearly impossible to provide a complete review of this huge body of work, we try to pull out the most important concepts towards achieving high practical specific energy and long cycle-life. In particular, regarding the discussion on high specific energy devices, we specifically focus on papers published in the last 3 years which disclose the active material loading (in mg S cm^{-2} or related units).[12–41,64–69] This allows us to estimate practical performance metrics in an attempt to pinpoint the most promising routes towards achieving high practical specific energy and power.

2. Projecting the Practical Specific Energy of a Li-S Cell

Estimating the specific energy (typically expressed in Wh kg^{-1}) or power (in kW kg^{-1}) of a battery requires knowledge of the mass of all battery components, not only the active material in the cathode or anode. In general, a rule of thumb for battery technologies is to divide the theoretical specific energy (E^*) by a factor of 3 to account for these other components.[6] However, the fact that Li-S prototypes exhibiting only 350 Wh kg^{-1} compared to the 2567 Wh kg^{-1} theoretically available suggests that this correction factor must be much larger than 3 (≈8 in this case). To better understand this and to assess current progress towards improvements to Li-S battery development, we define some design parameters and assumptions in an attempt to estimate this correction factor which allows us to put everyone's work on the same page (at least to a first approximation).

Table 1. Approximate mass of cell components that scale with active material loading.

Cell component	$f_{\infty,i}$ [mg mg^{-1}][a]	
	Li-S case	Li-ion case
Electrolyte	0.43	0.35
Binder (10 wt%)	0.17	0.11
Conductive additive	0.50	0.03
Cathode material	1.00	1.00
Anode material	–	0.43
Total f_∞	2.10	1.92

[a]Assumptions: Ratio of active material to conductive additive assumed to be 2 for Li-S case and 30 for Li-ion case; A stoichiometric amount of graphite anode was assumed in Li-ion case; Cathode porosity – $\varepsilon = 0.35$ used to calculate electrolyte mass; Electrolyte density = 0.97 g cm^{-3}, which is an average of pure DOX and DOL; Carbonaceous material density = 2.2 g cm^{-3}; Binder density (PTFE) = 1.78 g cm^{-3}.

2.1. Parameterizing Li-S Battery Components

Table 1 and **Table 2** list the various components of a full battery cell and separates them into two categories: i) components with mass that scales with the loading of active material ($f_{\infty,i}$ in mg mg^{-1} active material) such as the binder or conductive additive that is mixed in a specified ratio with the anode or cathode and ii) components with fixed mass ($f_{0,i}$) such as the current collectors and membrane separator. The electrolyte is often one of the most significant mass fractions and must be distributed between both of these categories and is estimated by the mass required to fill the void fraction (ε) in both the electrode materials and membrane separator. The amount of anode material required to balance the capacity of the cathode must also be taken into account. For example, by balancing the charge of the anode and cathode it can be shown that $f_{\infty,Li} = Q_{sulfur}/Q_{lithium} =$ 0.43 mg Li per mg S. This would provide the minimum amount of Li metal necessary to balance the sulfur. However, due to SEI formation and Li degradation with cycling a significant excess (>100–200%) of Li is often required. Furthermore, thin films of Li metal would require a current collector (typically Cu foil) for support while thicker films could potentially act as a current collector themselves. In an alternative strategy, the metal anode may be used in excess, at constant thickness, and in a form that is commercially available, such as the 125 µm foils produced by FMC Corp., which would then be a component of f_0 and not f_∞. Such a situation would enable the Li metal to act as both active anode material and current collector replacing the heavy Cu current collectors used to support the graphite anodes of most Li-ion batteries. Of course, the particular case depends on the final battery design. For the purposes of this review we chose to compare results assuming a Li foil with set thickness was used which can be translated to a mass density by multiplying the thickness (δ) and density (ρ) of Li metal (i.e., $f_{0,Li} \propto \delta\rho$). We will discuss the differences between the various anode design options and their impact on our analysis in the next section. Commonly used assumptions were used to determine the parameters listed in Table 1 and 2. For example, a void fraction or porosity of $\varepsilon = 0.35$ is assumed as this is in the range of what is commonly assumed or reported for commercial Li-ion electrodes ($\varepsilon = 0.25$–0.4).[70–72] However, we will later discuss that this may be a significant underestimate of the porosity for many sulfur-based cathode designs. We chose to assume a 16 µm thick Al foil, as any thinner foils have supposedly been found not mechanically robust enough for high throughput manufacturing.

Table 2. Approximate mass density of battery cell components that do not scale with active material loading.

Cell component	$f_{0,i}$ (mg cm^{-2})[a]	
	Li-S case	Li-ion case
Al current collector	4.3	4.3
Membrane separator	1.0	1.0
Electrolyte in membrane	1.3	1.3
Anode material	6.7	–
Cu current collector	–	9.9
Total f_0	13.4	16.5

[a]Assumptions: 25 µm polypropylene (density = 0.91g/cm^3) membrane with a porosity of 55% was assumed to calculate mass of electrolyte in separator; 16 µm thick Al foil current collector; 11 µm thick Cu foil current collector; Electrolyte density same as Table 1; 125 µm Li – metal anode for Li-S case.

Approximate values for f_∞ and f_0 (such as those reported in Table 1 and 2) as well as the loading of active material (t in mg cm^{-2}) can then be used to estimate the fraction of cathode active material (F) in a full battery using a simple mass balance:

$$F = \frac{\text{mass active material}}{\text{total mass}} = \frac{t}{f_\infty t + f_0} \quad (1)$$

This can be used to estimate the corrected, practical, specific energy (E)[73] if the cathode capacity and approximate average cell potential (U) are known, according to:

$$E = FQ_cU \quad (2)$$

2.2. Sensitivity Analysis

This formalism allows us to probe the sensitivity of E to changes in electrode formulation. As discussed above, the main difference between the Li-S system and many Li-ion batteries is the insulating nature of sulfur which, in most cases, requires the battery scientist/engineer to add much more conductive additive in order to mitigate the resistive losses in the system that preclude both high active material loadings and reasonable charge/discharge times. Electronically conducting cathode materials such as $LiCoO_2$ and $LiFePO_4$ can be made into thick films with very little (3–5 wt%)[71] conductive carbon additive, while the mass fraction of carbonaceous materials in Li-S batteries is often much larger as illustrated in **Figure 3** which summarizes the fraction of sulfur in the cathodes used in over 80 publications as surveyed by Hagen et al.[33] As discussed in more detail in Section 3, sulfur cathodes maintain their capacity at only a fraction of the mass loadings achieved by most Li-ion battery cathodes.

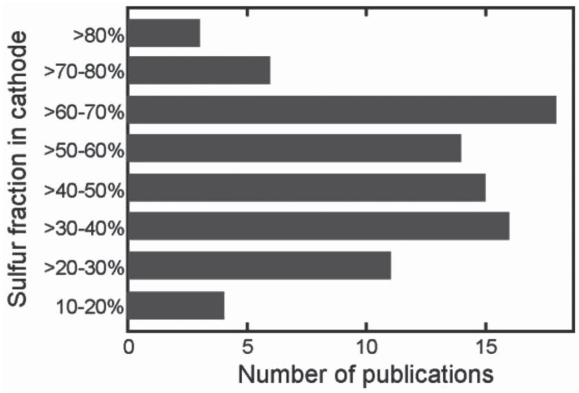

Figure 3. Fraction of sulfur in cathodes as a function of publication number (n = 87). Adapted with permission.[33] Copyright 2013, Elsevier.

Figure 4 illustrates how F and E progress as a function of active material loading for both the Li-S system and a Li-ion battery based on $LiCoO_2$ using the parameters estimated in Table 1 and 2. While different values of f_0 and f_∞ were used for the two different cases, the dependence of F on active material loading is largely the same. We also plot the Li-S case if a larger value of $\varepsilon = 0.5$ is assumed and show that the difference between the two cases is small at low loadings (<5 mg cm^{-2}), but becomes much more significant at higher loadings. Two limiting cases are highlighted. When the loading is small, $F \rightarrow f_0^{-1}$ and thus F and E do not depend strongly on the fraction of conductive additive or binder. On the other hand, at high loadings, the situation is reversed and F approaches a limit dictated mainly by the fraction of these components (i.e., $F \rightarrow f_\infty^{-1}$). State-of-the-art Li-ion battery technologies are engineered with cathodes exhibiting $t \approx$ 15–25 mg cm^{-2} in order to reach the latter limit.[33,35,41] Most academic work on Li-S batteries, use cathodes with t ≈ 1–4 mg S cm^{-2} and by reading off Figure 4b, the reported specific energy of prototype cells (350 Wh kg^{-1}) may also lay within this range. In the majority of cases, for Li-S batteries, F is so small that E does not exceed values which could be achieved by optimized Li-ion batteries. From this analysis, it appears that the most important criterion for improving E for the Li-S system is to maintain high Q_C at higher t. The fact that we are in the low loading limit suggests that the optimization process used to maximize E will be less sensitive to the fraction of conductive additive and more sensitive to the achievable capacity and active material loading.

As discussed in the previous section, there were several options to choose from regarding the anode design: i) Some excess of the stoichiometric amount of Li-metal (150% excess is assumed here); ii) Constant Li-metal thickness or iii) a stoichiometric amount of Li-metal supported by a Cu foil current collector. In **Figure 5**, we plot F for these three cases as a function of S loading while holding all other parameters constant. Clearly the mass of even a thin Cu foil (11 µm) significantly reduces F and thus the specific energy while the stoichiometric excess of Li-metal appears to be the best case scenario. In practice, it is likely that thin films of Li-metal would also require support from a current collector and thus, for the analysis in this review, we chose to use the intermediate case ii) where a 125 µm thick foil is assumed. This assumption also provides the smallest deviation between the two possible extremes of anode design. Of course, the actual design chosen would depend on the performance, manufacturability and economics and would also need to include any protective or passivation layers which may be required to prevent or slow Li-metal degradation.

In our analysis, we have not included the contribution of packaging as this depends largely on packaging type, size and the application which may require the battery to have protective shielding or safety devices. The fractional mass of packaging can be made negligible by manufacturing batteries with many layers. In multilayer cells it is also possible to coat each current collector foil on both sides which reduces the mass of Al or Cu foil by a factor of 2. On the other hand, battery packs, for example, designed for electric vehicles, must contain safety features, control systems and support structures that can lead to significant mass increases over just the batteries themselves. While we will not discuss pack level design, such factors could in principle also be included in F to estimate the practical, specific energy of a battery pack.

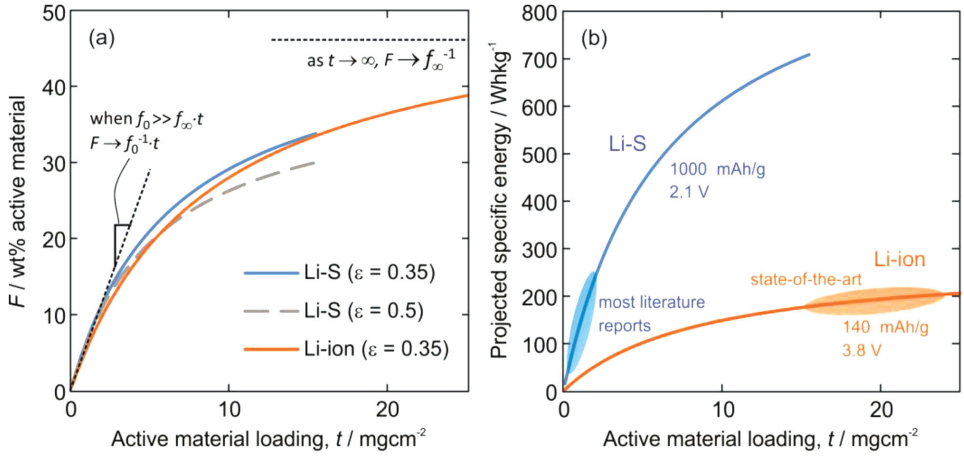

Figure 4. Estimating the practical specific energy of a Li-S cell. a) Fraction of active material in a full battery. (b) Corresponding practical energy density calculated as $E = FQ_CU$ as a function of active material loading and several assumed parameters (see Table 1, 2). For the sulfur case, the assumption that a 125 µm thick Li foil was used required us to stop the curve at ≈15.6 mg cm^{-2} as this corresponds to the point where Li metal is no longer in excess.

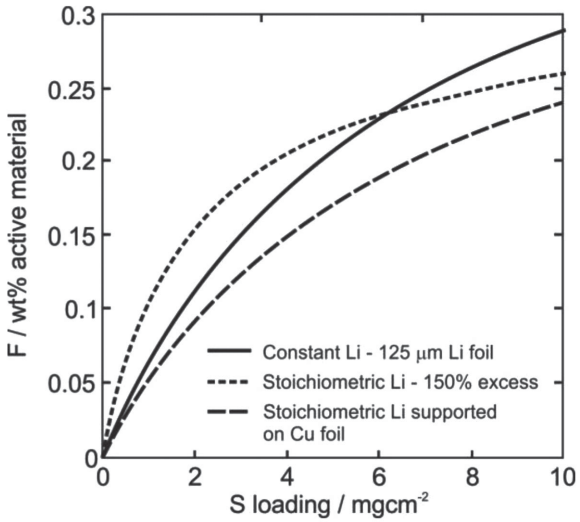

Figure 5. Effect of assumed anode configuration on *F*. For the Cu current collector case, an 11 μm thick Cu foil was assumed. Variations in *F* as large as 25% between the 3 cases leads to a significant uncertainty in the absolute value of the specific energy we estimate.

3. Sulfur Cathode Architectures

The analysis described above was applied to experimentally determined capacities at various rates, active material loadings and fractions of conductive additive by extracting this information from work published over the past 3 years (2012, 2013, and 2014). These data are compiled in **Table 3** and were used to estimate *F*, *E* and an approximate average specific power, P_{avg} in order to draw conclusions about the efficacy of various cathode architectures and materials. The following sections break these results into four categories: i) Conventional approaches amenable to typical battery manufacturing based on casting the cathode material and conductive additive onto a current collector such as Al foil. ii) Approaches which embed the cathode material into less conventional, thick, 3D current collectors. iii) All solid-state Li-S batteries and iv) systems based on a liquid-phase cathode which are commonly referred to as catholytes.

3.1. Conventional Approach: 2D Current Collectors

Most batteries are prepared by some method of casting, pressing or calendaring a mixture of active material, binder and conductive additive onto a thin Al or Cu foil current collector.[74] The metallic foil provides sufficient conductivity to allow for a battery to be wound many times in its cell without significant resistive losses. It also minimizes the current that has to flow through a short distance within the less conductive, solid, active material matrix which typically extends several tens of micrometers in thickness outwards from the surface of the current collector. Most approaches for preparing sulfur cathodes use this design and are discussed in this section. Literature data are compiled for this configuration and reported in Table 3.

Most frequently, carbonaceous material are used as the conductive additive. Many allotropes of carbonaceous materials have been used for this purpose such as activated carbons,[26–28] carbon blacks,[19–22,24,25] carbon nanotubes,[18,23,29] and graphene,[12–18] which exhibit high specific surface area, high electrical conductivity and good thermal and chemical stability. Other materials used include conductive polymers such as polyaniline,[39,75] metal oxides,[44–49] and, more recently, metal organic frameworks.[50,51] The motivation for choosing some of these materials also comes from the various interactions and ability to confine the soluble polysulfide species formed while cycling Li-S batteries in liquid phase electrolytes.

Various approaches have been employed to distribute sulfur on or within these high specific surface areas, conductive supports in order to improve electronic transport to and from this insulating material. These approaches have been described in several recent reviews[76,77] and thus we will only highlight some of the generally used schemes here. Common sulfur deposition approaches involve melt imbibing sulfur into the carbonaceous host,[44] precipitating sulfur from elemental sulfur dissolved in solvents such as carbon disulfide[78] or chemical reactions with various sulfur precursors such as $Na_2S_2O_3$.[29] The optimization of such strategies has led to cathodes which exhibit very high initial capacities (>1400 mAh g^{-1} S)[12,26,29,32] approaching the expected theoretical capacity of 1672 mAh g^{-1} S. Unfortunately, the capacity typically drops in subsequent cycles for a variety of reasons which will be discussed further in Sections 4–6.

In **Figure 6** we have plotted the projected specific energy as a function of sulfur loading (at various rates) and as a function of power density (for various loadings) from the values tabulated in Table 3. Before the results of this analysis are discussed further we would like to emphasize the assumptions made. While the tabulated results were obtained using various electrolytes, additives, cathodes with various void fractions (not typically specified), anodes and anode thicknesses etc. we have normalized all results to the same set of criteria. The mass loading of binder, Al foil, membrane, Li foil, electrolyte density and void fraction were held constant for all comparisons while the reported ratio of sulfur to conductive additive (S:A), sulfur loading and capacity were used as adjustable parameters for the different reported charge/discharge rates. The average cell voltage was also held constant at 2.1 V. This is an overestimate at high current densities where various cell resistances may cause significant voltage drop. As argued above, these calculations are not very sensitive to minor changes in the battery design criteria assumed (electrolyte type and thus density, binder fraction, void fraction, etc.) especially at the lower loadings (<5 mg cm^{-2}) we discuss.

As shown in Figure 6, at sulfur loadings less than 2 mg S cm^{-2}, almost none of the reported capacities lead to *E* significantly higher than what could be achieved by current Li-ion technologies. In this loading regime, there is an approximately linear correlation of *E* with loading which is more apparent if results of similar current density are plotted (not shown). The maximum estimated specific energies are achieved at ≈4 mg S cm^{-2}, closely approaching 500 Wh kg^{-1} at charge/discharge times exceeding ≈10 h. These high values have been achieved using functionalized graphene sheets (FGSs) obtained by thermally exfoliating graphite oxide,[79] multiwalled carbon nanotubes (MWCNTs),[29] polyaniline,[80] and using covalently bound sulfur-polymer composites based on sulfurized-polyacrylonitrile (S-PAN).[81,82]

From our estimates, one of the highest performing Li-S cells was reported by Su et al. who prepared so-called self-weaving

Table 3. Summary of literature data and estimates of E and P for conventional sulfur-based electrodes cast on Al foil current collectors as a function of additive type.

Cond. additive/ type	$S:A$[a)] ratio [wt/wt]	t [mg S cm^{-2}]	C-rate [h^{-1}]	j [mA cm^{-2}]	Q_Cb) [mAh g^{-1} S]	Q_{areal} [mAh cm^{-2}]	f_∞ [mg Mg^{-1} S]	f_0 [mg cm^{-2}]	F [mg S mg^{-1}]	E [Wh kg^{-1}]	P_{avg}[c)] [W kg^{-1}]	Ref.
FGS /polypyrrol	0.86	2.0	0.1	0.34	1415.7	2.83	3.0	13.4	0.10	314	37	[12]
	0.86	2.0	0.5	1.68	988.7	1.98	3.0	13.4	0.10	219	186	
	0.86	2.0	1	3.35	830.1	1.66	3.0	13.4	0.10	184	372	
FGS	0.96	1.0	3.8	6.05	794	0.75	2.8	13.4	0.059	101	809	[13]
FGS	2.85	1.0	0.1	0.17	1240	1.24	1.9	13.4	0.07	175	24	[14]
	2.85	1.0	0.5	0.84	967.2	0.97	1.9	13.4	0.07	136	118	
	2.85	1.0	1	1.68	582.8	0.58	1.9	13.4	0.07	82	236	
	2.85	1.0	2	3.35	471.2	0.47	1.9	13.4	0.07	66	472	
FGS/phenolic resin	2.21	0.7	0.25	0.31	1000	0.74	2.0	13.4	0.05	107	45	[15]
	2.21	0.7	0.5	0.62	850	0.63	2.0	13.4	0.05	91	89	
	2.21	0.7	1	1.24	750	0.56	2.0	13.4	0.05	80	179	
	2.21	0.7	2	2.47	700	0.52	2.0	13.4	0.05	75	358	
	2.21	0.7	5	6.19	600	0.44	2.0	13.4	0.05	64	895	
FGS/cellulose	0.84	2.0	0.1	0.33	1200	2.40	3.0	13.4	0.10	265	37	[16]
FGS/mesoporous carbon	7.95	1.5	0.2	0.50	1170	1.76	1.6	13.4	0.10	240	69	[17]
	7.95	1.5	0.5	1.25	700	1.05	1.6	13.4	0.10	143	171	
	7.95	1.5	1	2.51	650	0.98	1.6	13.4	0.10	133	343	
FGS and MWCNTs	2.46	0.9	1	1.42	1200	1.02	2.0	13.4	0.06	146	203	[18]
	2.46	0.9	2	2.84	920	0.78	2.0	13.4	0.06	112	407	
	2.46	0.9	3	4.26	850	0.72	2.0	13.4	0.06	103	610	
	2.46	0.9	5	7.11	750	0.64	2.0	13.4	0.06	91	1016	
FGS (Vor-XTM)	1.25	4.4	0.06	0.44	1258.9	5.53	2.5	13.4	0.18	487	39	NA
	1.25	4.4	0.12	0.88	1178.6	5.17	2.5	13.4	0.18	456	77	
	1.25	4.4	0.2	1.46	1142.5	5.02	2.5	13.4	0.18	442	129	
	1.25	4.4	0.6	4.39	1074.7	4.72	2.5	13.4	0.18	416	387	
	1.25	4.4	1.2	8.78	986.8	4.33	2.5	13.4	0.18	382	774	
	1.25	3.4	0.06	0.34	1471	4.95	2.5	13.4	0.15	488	33	
	1.25	3.4	3	16.8	786.3	2.65	2.5	13.4	0.15	261	1659	
	1.25	3.4	6	33.7	185.8	0.63	2.5	13.4	0.15	62	3317	
	1.25	3.4	9	50.5	9.489	0.03	2.5	13.4	0.15	3	4976	
Carbon black	2.96	1.5	0.1	0.25	1120	1.68	1.9	13.4	0.09	223	33	[19]
	2.96	1.5	0.5	1.26	795	1.19	1.9	13.4	0.09	159	167	
	2.96	1.5	1	2.51	720	1.08	1.9	13.4	0.09	144	334	
	2.96	1.5	2	5.03	630	0.95	1.9	13.4	0.09	126	668	
	2.96	1.5	3	7.54	590	0.89	1.9	13.4	0.09	118	1002	
	2.96	1.5	4	10.1	560	0.84	1.9	13.4	0.09	112	1336	
	2.96	1.5	5	12.6	540	0.81	1.9	13.4	0.09	108	1670	
Carbon black (KB)	1.17	0.5	0.1	0.09	1360	0.73	2.6	13.4	0.04	107	13	[20]
	1.17	0.5	0.2	0.18	700	0.38	2.6	13.4	0.04	55	26	
	1.17	0.5	1	0.90	500	0.27	2.6	13.4	0.04	39	131	
Carbon black (KB)	0.62	5.0	0.06	0.50	753.8	3.77	3.6	13.4	0.16	257	34	[21]
	0.62	5.0	0.31	2.50	580	2.90	3.6	13.4	0.16	198	170	

Continued

Table 3. Continued

Cond. additive/ type	*S*:*A*[a] ratio [wt/wt]	*t* [mg S cm^{-2}]	C-rate [h^{-1}]	*j* [mA cm^{-2}]	Q_Cb) [mAh g^{-1} S]	Q_{areal} [mAh cm^{-2}]	f_∞ [mg Mg^{-1} S]	f_0 [mg cm^{-2}]	*F* [mg S mg^{-1}]	*E* [Wh kg^{-1}]	P_{avg}[c)] [W kg^{-1}]	Ref.
Carbon black (KB)	2.00	1.2	0.09	0.17	740	0.89	2.1	13.4	0.08	120	23	[22]
	2.00	1.2	0.13	0.25	680	0.82	2.1	13.4	0.08	110	34	
	2.00	1.2	0.26	0.50	530	0.64	2.1	13.4	0.08	86	68	
	2.00	1.2	0.52	1.00	390	0.47	2.1	13.4	0.08	63	136	
	2.00	1.2	1.04	2.00	200	0.24	2.1	13.4	0.08	32	271	
Denka black/ MWCNTs	1.45	0.4	0.02	0.01	1150	0.43	2.4	13.4	0.03	65	2	[23]
	1.45	0.4	0.1	0.06	795	0.30	2.4	13.4	0.03	45	9	
	1.45	0.4	0.2	0.13	570	0.21	2.4	13.4	0.03	32	19	
	1.45	0.4	0.5	0.31	350	0.13	2.4	13.4	0.03	20	47	
Super-P	2.00	1.5	0.2	0.50	804	1.21	2.1	13.4	0.09	157	65	[24]
Super-P	5.33	3.0	0.04	0.20	1049	3.15	1.7	13.4	0.16	369	23	[25]
	5.33	3.0	0.04	0.20	965	2.90	1.7	13.4	0.16	339	23	
Carbide-derived carbon	1.38	1.0	0.1	0.17	1450	1.45	2.4	13.4	0.06	198	23	[26]
	1.38	1.0	0.2	0.34	1370	1.37	2.4	13.4	0.06	187	46	
	1.38	1.0	0.5	0.84	1295	1.30	2.4	13.4	0.06	177	114	
	1.38	1.0	1	1.68	1190	1.19	2.4	13.4	0.06	162	228	
	1.38	1.0	0.1	0.17	1040	1.04	2.4	13.4	0.06	142	23	
	1.38	1.0	0.2	0.34	950	0.95	2.4	13.4	0.06	130	46	
	1.38	1.0	0.5	0.84	770	0.77	2.4	13.4	0.06	105	114	
	1.38	1.0	1	1.68	640	0.64	2.4	13.4	0.06	87	228	
	1.38	1.0	0.1	0.17	750	0.75	2.4	13.4	0.06	102	23	
	1.38	1.0	0.2	0.34	610	0.61	2.4	13.4	0.06	83	46	
	1.38	1.0	0.5	0.84	510	0.51	2.4	13.4	0.06	70	114	
	1.38	1.0	1	1.68	405	0.41	2.4	13.4	0.06	55	228	
Activated carbon	2.60	0.5	0.1	0.08	1300	0.65	1.9	13.4	0.03	98	13	[27]
	2.60	0.5	0.2	0.17	950	0.48	1.9	13.4	0.03	71	25	
	2.60	0.5	1	0.84	600	0.30	1.9	13.4	0.03	45	126	
N-doped, Mesoporous	3.50	4.2	0.1	0.70	800	3.36	1.8	13.4	0.20	345	72	[28]
Carbon PEDOT	2.57	1.7	0.13	0.33	1040	1.73	1.9	13.4	0.10	224	43	[37]
	2.57	1.7	0.25	0.66	980	1.63	1.9	13.4	0.10	211	86	
	2.57	1.7	0.5	1.33	940	1.56	1.9	13.4	0.10	202	172	
	2.57	1.7	1	2.66	900	1.49	1.9	13.4	0.10	194	344	
Polypyrrole	1.37	4.0	0.06	0.40	1320	5.28	2.4	13.4	0.17	493	37	[38]
Polyaniline	0.51	3.0	3	14.3	1060	3.16	4.1	13.4	0.12	265	1205	[39]
	0.51	3.0	5	23.9	705	2.10	4.1	13.4	0.12	177	2008	
	0.51	3.0	10	47.8	410	1.22	4.1	13.4	0.12	103	4016	
MWCNTs	0.67	1.6	1	2.65	1420	2.24	3.5	13.4	0.08	256	302	[29]
	0.67	1.6	2	5.29	1290	2.04	3.5	13.4	0.08	232	604	
	0.67	1.6	3	7.94	1120	1.77	3.5	13.4	0.08	202	905	
	0.67	1.6	4	10.59	1080	1.71	3.5	13.4	0.08	195	1207	
	0.67	1.6	0.5	1.32	1030	1.63	3.5	13.4	0.08	186	151	
	1.70	4.0	0.5	3.4	1050	4.23	2.2	13.4	0.18	408	325	
	1.70	4.0	1	6.8	950	3.83	2.2	13.4	0.18	369	651	
	1.70	4.0	2	13.5	850	3.43	2.2	13.4	0.18	330	1302	
Carbon fibers	0.98	0.9	0.1	0.15	980	0.87	2.8	13.4	0.06	118	20	[30]
	0.98	0.9	0.02	0.03	1200	1.07	2.8	13.4	0.06	145	4	

Continued

Table 3. Continued

Cond. additive/ type	*S:A*[a] ratio [wt/wt]	*t* [mg S cm^{-2}]	C-rate [h^{-1}]	*j* [mA cm^{-2}]	Q_C[b] [mAh g^{-1} S]	Q_{areal} [mAh cm^{-2}]	f_∞ [mg Mg^{-1} S]	f_0 [mg cm^{-2}]	*F* [mg S mg^{-1}]	*E* [Wh kg^{-1}]	P_{avg}[c] [W kg^{-1}]	Ref.
Carbon fibers (hollow)	1.18	1.5	0.2	0.50	1200	1.80	2.6	13.4	0.09	225	63	[31]
	1.18	1.5	0.5	1.3	800	1.20	2.6	13.4	0.09	150	156	
	1.18	1.5	1	2.5	680	1.02	2.6	13.4	0.09	127	313	
	1.18	1.5	2	5.0	600	0.90	2.6	13.4	0.09	112	626	
Sulfurized-PAN	0.63	5.0	0.03	0.25	1405	7.02	3.6	13.4	0.16	482	17	[32]
	0.55	5.0	0.03	0.25	896	4.48	3.9	13.4	0.15	292	16	
	0.40	5.0	0.03	0.25	785	3.93	4.9	13.4	0.13	223	14	
	0.30	5.0	0.03	0.25	110	0.55	6.0	13.4	0.12	27	12	
Sulfurized-PAN	0.51	0.6	0.2	0.18	1050	0.58	4.1	13.4	0.04	79	25	[40]
	0.51	1.2	0.2	0.40	1050	1.26	4.1	13.4	0.07	148	47	
	0.51	1.8	0.2	0.60	1050	1.89	4.1	13.4	0.09	196	62	
	0.51	2.3	0.2	0.77	1050	2.42	4.1	13.4	0.10	227	72	
	0.51	3.1	0.2	1.04	1050	3.26	4.1	13.4	0.12	268	85	
	0.51	4.1	0.2	1.37	1050	4.31	4.1	13.4	0.14	306	98	
	0.51	5.2	0.2	1.74	1050	5.46	4.1	13.4	0.15	338	108	
	0.51	5.9	0.2	1.97	1050	6.20	4.1	13.4	0.16	354	113	
	0.51	1.2	1	2.01	850	1.02	4.1	13.4	0.07	120	236	
	0.51	2.3	1	3.85	800	1.84	4.1	13.4	0.10	173	362	
	0.51	3.1	1	5.18	650	2.02	4.1	13.4	0.12	166	427	
	0.51	5.9	1	9.86	375	2.21	4.1	13.4	0.16	126	563	
TiS	0.55	3.7	0.02	0.10	810	3.00	3.9	13.4	0.13	232	8	[49]
	0.55	3.7	0.05	0.30	600	2.20	3.9	13.4	0.13	170	23	
	0.55	3.7	0.1	0.60	430	1.60	3.9	13.4	0.13	124	46	

[a]*A* refers to the additive used to improve electrical conductivity; [b]In many cases Q_C was estimated from a graphical representation and thus values may be off by ± 10 mAh g^{-1}; [c]P_{avg} was estimated by dividing *E* by the timescale of charge/discharge estimated by dividing the capacity (in mAh g^{-1}) by the rate (in mA g^{-1}).

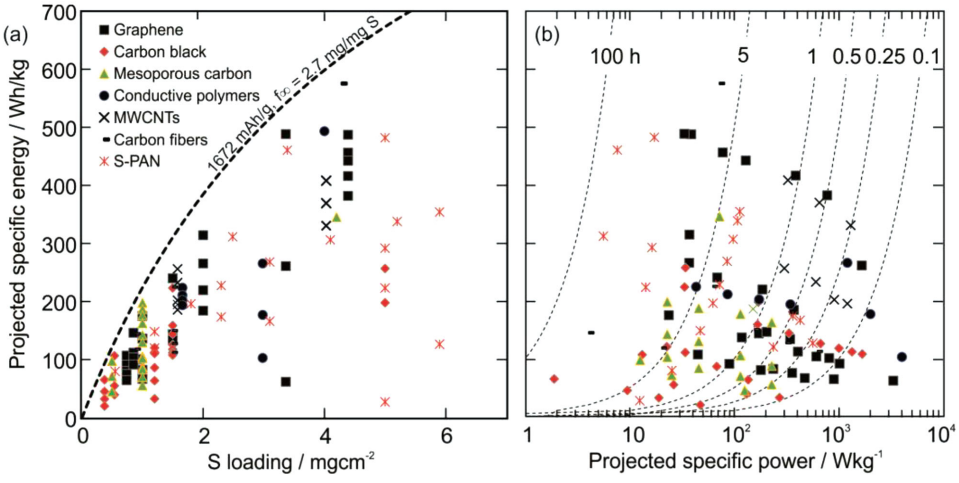

Figure 6. Projected specific energy of various literature reports using traditional 2D current collectors. a) *E* as a function of S loading; b) *E* as a function of P_{avg} for cathodes embedded in 3D current collector structures. Dashed line in (a) indicates *E* if a cathode displayed the theoretical capacity of sulfur with f_∞ = 2.7 mg (mg S)$^{-1}$ and f_0 = 13.4 mg cm^{-2}. Dashed lines in (b) indicate lines of the constant charge/discharge rate estimated using the approximate timescale, $\tau = E/P_{avg}$.

sulfur-MWCNT composite cathodes. The composites were prepared by dispersing MWCNTs with Triton X-100, coating the CNTs with sulfur through reaction between $Na_2S_2O_3$ and HCl followed by vacuum filtration to yield flexible, free-standing films. Their high loading films (≈4 mg S cm^{-2}) were tested at relatively high C-rates (0.5–2C) and demonstrated impressive capacities. Our estimates indicate that such films could be made into full cells with E ≈ 410 Wh kg^{-1} for the C/2 case, which, by our estimates, represents the highest specific energy at high specific power reported in the recent literature. While these estimates are based on 10 wt% binder and an Al foil current collector, the authors claim that these components are unnecessary for their system. Removing these mass components from our analysis would lead to ≈530 Wh kg^{-1}.

We have also included our own data obtained for optimized Li-S cells developed by Vorbeck Materials Corp.[79] For these cells, FGSs were mixed with sulfur to prepare cathodes with high sulfur loading (data for 3.4 and 4.4 mg S cm^{-2} are reported in **Table 4**). These electrodes were able to achieve outstanding capacity at high rates. At C/10 we estimate that the specific energy approaches 500 Wh kg^{-1} and at high rates these electrodes achieve similar performance to the results demonstrated for MWCNTs. At extreme rates of 5C, the projected *E* maintains a value higher than what has been achieved with optimized Li-ion systems at slow charge/discharge rates. We also estimate that two other works based on conductive polymers could also achieve high specific energy but only at slower rates (slower than C/10).[80] Zhang et al. prepared sulfur/polypyrrole composites by a simple ball milling

Table 4. Summary of literature data and estimates of *E* and P_{avg} for sulfur-based electrodes based on various 3D current collector designs.

3D current collector material	S/A ratio[a)]	*t* [mg cm^{-2}]	C-rate [h^{-1}]	*j* [mA cm^{-2}]	Q_C b) [mAh g^{-1}]	Q_{areal} [mAh cm^{-2}]	f_∞ [mg mg^{-1}]	f_0 [mg cm^{-2}]	*F* [%]	*E* [Wh kg^{-1}]	P_{avg}[c)] [W kg^{-1}]	Ref.
Carbon fiber/ embedded CNTs	0.53	5.8	0.07	0.64	1110	6.4	3.98	21.9	13	308	31	[33]
	0.54	5.9	0.06	0.64	1110	6.5	3.94	21.9	13	312	31	
	1.45	16	0.02	0.64	800	12.8	2.35	17.5	29	499	25	
	2.22	8	0.05	0.64	1010	8.1	2.03	17.5	24	514	41	
	0.84	9.2	0.04	0.64	1170	10.8	3.04	17.5	20	509	30	
	1.11	12.2	0.03	0.64	900	11.0	2.64	17.5	25	475	28	
	1.43	15.7	0.02	0.64	805	12.6	2.37	17.5	29	496	25	
	2.22	8	0.10	1.28	900	7.2	2.03	17.5	24	458	81	
	0.84	9.2	0.08	1.28	805	7.4	3.04	17.5	20	350	61	
	1.11	12.2	0.06	1.28	770	9.4	2.64	17.5	25	406	55	
	1.43	15.7	0.05	1.28	580	9.1	2.37	17.5	29	358	50	
	2.22	8	0.19	2.56	835	6.7	2.03	17.5	24	425	163	
	0.84	9.2	0.17	2.56	780	7.2	3.04	17.5	20	339	121	
	1.11	12.2	0.13	2.56	680	8.3	2.64	17.5	25	359	111	
	1.43	15.7	0.10	2.56	480	7.5	2.37	17.5	29	296	101	
	1.11	12.2	0.19	3.84	600	7.3	2.64	17.5	25	316	166	
	1.43	15.7	0.15	3.84	375	5.9	2.37	17.5	29	231	151	
Al foam/ embedded CNTs	1.00	7	0.10	1.17	860	6.0	2.77	14.1	25	386	75	[41]
	1.00	12.5	0.10	2.09	642	8.0	2.77	14.1	21	354	92	
	1.00	12.5	0.20	4.18	634	7.9	2.77	14.1	26	349	184	
	1.00	12.5	0.50	10.45	507	6.3	2.77	14.1	26	279	460	
	1.00	12.5	1.00	20.9	347	4.3	2.77	14.1	26	191	921	
Carbon nanofibers	0.25	0.5	0.06	0.05	1600	0.8	6.81	10.5	26	123	8	[34]
	1.13	1.7	0.06	0.17	1250	2.1	2.62	10.5	4	305	24	
	1.86	2.6	0.06	0.26	1000	2.6	2.15	10.5	11	347	35	
Graphene foam	1.08	2	0.48	1.61	800	1.6	2.67	13.4	16	184	185	35
	1.08	2	1.90	6.35	450	0.9	2.67	13.4	11	103	731	
	4.00	11.9	0.10	1.99	504	6.0	1.76	12.0	11	391	130	
Carbon cloth	0.70	13	0.02	0.5	645	8.38	3.37	13.4	36	315	18	[36]
	0.93	13	0.02	0.5	778	10.11	2.88	13.4	23	427	21	

[a)] *A* refers to the additive used to improve electrical conductivity.[b)] In many cases Q_C was estimated from a graphical representation and thus values may be off by ± 10 mAh g^{-1}; [c)] P_{avg} was estimated by dividing *E* by the timescale of charge discharge estimated by dividing the capacity (in mAh g^{-1}) by the rate (in mA g^{-1}).

approach.[80] Using electrodes with a loading of 4 mg S cm^{-2}, they were able to achieve high capacity (1320 mAh g^{-1}) which we estimate leads to $E \approx 490$ Wh kg^{-1} at ≈C/15. Wang et al. also reported high loading work for a different type of cathode material referred to as S-PAN.[32] Heating sulfur in the presence of polyacryolnitrile (PAN) forms a molecular composite material where sulfur is covalently bound to the dehrydrogenated PAN backbone.[17,75,83] As will be discussed in later sections, this material also promotes stable cycling. We estimate that the specific energy of the reported high loading (5 mg S cm^{-2}), high capacity (1400 mAh g^{-1}) cathode could achieve ≈480 Wh kg^{-1} at very slow charge/discharge rates. These authors fabricated a 100 mAh prototype battery from their material and claim to achieve a practical specific energy of 437 Wh kg^{-1} (not including packaging and using 80% excess Li metal), which is close to our estimate.

From these reports it seems quite feasible that a 450–500 Wh kg^{-1} battery can be fabricated from a variety of sulfur-based cathodes. However, high rate performance (faster than C/2), has only been demonstrated for high surface area, highly conductive nanomaterials such as FGSs[79] or MWCNTs.[29] From the limited data available at high loadings it is difficult to determine whether or not other materials could also achieve such exceptional performance.

The lack of research carried out with high S loading is likely a result of the difficulty in fabricating thick, sulfur-based electrodes, especially when using high surface area carbonaceous materials. It is technically challenging to fabricate such cathodes by traditional approaches for several reasons: i) Both sulfur and the carbonaceous materials typically used as the conductive additive are much lower in density (≈2 g cm^{-2}) compared to conventional Li-ion battery cathode materials (≈8–10 g cm^{-2}). For the same slurry mass loading, the slurry viscosity is much larger for the sulfur case, due to the larger volume of solids. Conversely, to achieve the same slurry viscosity required for successful casting, it is necessary to dilute the slurry which results in inhomogeneities through particle segregation and cracking due to excessive shrinkage, a common observation in ceramic materials processing.[84] ii) High aspect ratio carbonaceous materials such as graphene or CNTs also significantly increase the slurry viscosity especially at the high concentrations used in Li-S batteries. Thus, to effectively incorporate these materials into thick, dense sulfur cathodes, traditional coating approaches may need to be adapted or redesigned.

3.2. Cathodes Embedded in 3D Current Collectors

Over the last few years there has been an increasing number of reports which describe sulfur-based materials which are embedded into a variety of 3D current collectors made either from metal[41–43] or graphene foams,[35] and woven or non-woven mats of carbon fibers.[85,86] The motivation of these studies has been to improve the active material loading by mechanically embedding the cathode material into a 3D support matrix and also to reduce the effective distance electronic charge must travel between the current collector and thicker cathode films. A graphene foam is shown in **Figure 7** with various sulfur loadings (0, 3.3 6.1 and 10.1 mg S cm^{-2}). These SEM images also show the large amount of void space that typically

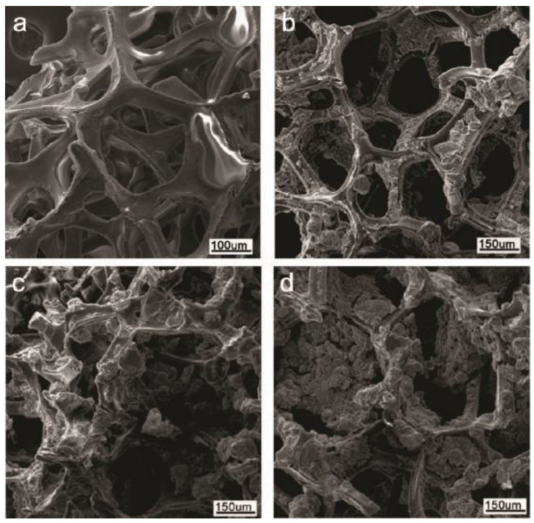

Figure 7. SEM images of graphene foam 3D current collectors with various sulfur loadings. a) Current collector without any S. b) 3.3 mg S cm^{-2}. c) 6.1 mg S/cm^2. d) 10.1 mg S cm^{-2}. Reproduced with permission. [47] Copyright 2015, Elsevier.

results from these structures which lead to the requirement of excess electrolyte and likely a significant deviation from the $\varepsilon = 0.35$ we have assumed in our analysis.

The highest mass loadings achieved to date were reported by Hagen et al.[33] who grew carbon nanotubes (CNTs) on a thick carbon fiber support. Sulfur was melt imbibed into this matrix and the authors were able to explore the performance of S cathodes with loadings as high as 15.7 mg S cm^{-2}. By taking into consideration the extra mass of their carbon fiber mat (8.5 mg cm^{-2}) and assuming that this would not require an additional Al foil current collector, we estimate that several of their compositions could achieve ≈500 Wh kg^{-1} at slow rates (>10 h charge/discharge or <30 W kg^{-1}) but the specific energy drops off rapidly at higher rates. An interesting approach taken by Zhang and Tran was to sandwich thick carbon cloth current collector with a thick sulfur mat to create a high loading cathode (≈13 mg S cm^{-2}).[36] During initial operation, the sulfur mat slowly dissolved and deposited on the carbon cloth leading to $E \approx 470$ Wh kg^{-1} at relatively low $P_{avg} \approx 20$ W kg^{-1}. This work illustrates that intimate mixing of carbon and sulfur is not necessarily required as the solubility of sulfur species enables its redistribution during cycling. However, as will be discussed later, this could negatively impact the electrode's mechanical properties and cycle-life.

Several of these reports have demonstrated the ability to achieve exceptionally high areal capacity (Q_{areal} in mAh cm^{-2}), a practical metric often used to compare the potential of a battery technology. As listed in Table 4, Q_{areal} values in the 5–15 mAh cm^{-2} range have been achieved,[33–36,41] significantly exceed traditional approaches which have so far been limited to $Q_{areal} \approx$ 4–6 mAh cm^{-2}.[32,39,40] However, despite a nearly three-fold increase in Q_{areal}, our estimations, shown in **Figure 8**, indicate that there is no significant increase in the projected E. This is because of the large fraction of current collector and/or conductive additive that takes up more than 50% of the cathode by weight (and volume). Based on our analysis, this added mass outweighs the advantages of achieving high loadings. A

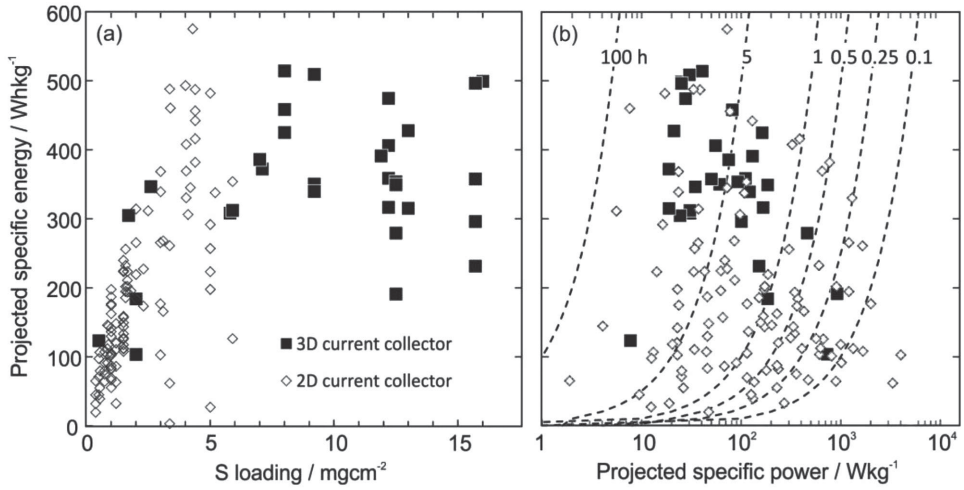

Figure 8. Comparing the projected specific energy of various literature reports using 3D current collectors to the more traditional 2D current collectors. a) E as a function of S loading; b) E as a function of P_{avg} for cathodes embedded in 3D current collector structures. Dashed lines in (b) indicate lines of the constant charge/discharge rate indicated estimated using the approximate timescale, $\tau = E/P_{avg}$.

side-effect of high loading and high Q_{areal} is the requirement to charge and discharge the battery at higher current densities (j) for the same C-rate. As will be discussed in Section 6, higher j typically leads to earlier failure of the Li metal anode. This was pointed out by Hagen et al.[33] who observed unstable cycling for their high loading cathodes due to frequent cell shorting caused by dendrite growth of Li metal across the membrane separator. We have also observed unstable cycling in our work when charging currents exceed a few mA cm^{-2}.

3.1.1. Effects of Porosity, Electrolyte Volume and Low S/C on Projected Energy Density

While we have assumed an electrode porosity of only $\varepsilon = 0.35$ throughout this review, it is clear that in most cases, this is a significant underestimate, especially with regard to 3D current collectors. As may be apparent by looking at Figure 7, this high porosity leads to a void fraction which is much larger than 0.35. Several studies have discussed the electrolyte content required to cycle these high porosity cathodes.[33] Hagen et al.,[33] mention a weight ratio of electrolyte to sulfur of 1.8 to 3 which is much larger than the 0.43 we estimated in Table 1. In other work, the interweaving MWCNT electrodes produced by Su et al. were reported to absorb 26 µL cm^{-2} of electrolyte which corresponds to a weight ratio of approximately 6.3 for their 4 mg S cm^2 cathodes. Even cathode materials deposited onto 2D current collectors likely suffer a low bulk density which results in excess void space. For example, Zheng et al. studied how the sulfur mass to electrolyte volume impacted the reproducibility of their measurements.[87] They found that a ratio of 50 g S L^{-1} electrolyte was optimum. This translates to ≈19.4 mg electrolyte/mg sulfur. In other work, Kang et al.[88] investigated the cycle stability of cathodes with various sulfur loadings (1–6.8 mg S cm^{-2}) with varying electrolyte amount added (2–40 µL mg^{-1} S). They found that they could achieve the most stable cycling at an electrolyte volume of 10 µL mg^{-1} S, which corresponds to an electrolyte to sulfur ratio of ≈10.

In order to illustrate how the excess porosity and electrolyte volume impact the projected specific energy, in **Figure 9**a we vary the fraction of electrolyte in our cathode and thus change f_∞ over the range of values of electrolyte to sulfur weight ratio reported in the literature. If these values are indeed required, it is clear from Figure 9a that the specific energy estimated in our previous analysis must be reduced by a factor of ≈40–60%, a deviation most significant at the high sulfur loadings used in the 3D current collector work. Reducing the electrolyte mass/volume required for cell operation will be critical to engineering batteries with the high specific energy estimated in Figure 6 and 8.

Furthermore, while we have not considered the volumetric energy density up to this point, it requires some attention as the variations in S/C and porosity between different reports can have a significant impact on this important practical metric. As discussed in §1, the volumetric energy density of a Li-S battery is not expected to be much higher than current Li-ion battery technologies due to the low density of S and Li metal. Using the assumed cell materials outlined in Table 1 and 2 we plot the maximum achievable volumetric energy density as a function of S/C and assumed porosity (i.e., ε) if the theoretical capacity of sulfur could be achieved. As shown in Figure 9b, for the parameters assumed, in the best case scenario, ≈600 Wh L^{-1} is just reached at ≈4 mg S cm^{-2}, which was near the optimum found for various works using 2D current collectors. Since the actual capacities as these loadings were below 1672 Wh kg^{-1} it is clear that Li-S cells will likely fall short of current Li-ion battery technologies which are known to achieve ≈600 Wh L^{-1}.[89] On the other hand, higher S loadings are possible with 3D current collectors. Unfortunately, the thick 3D current collectors lead to much smaller S/C ≈ 0.5–1 (see Table 4) and void fractions (not typically reported), which are presumably much larger than 0.35. The excessive void space and larger carbon content significantly reduces the maximum achievable volumetric energy density to the range which can be achieved by Li-ion batteries. Since the actual measured capacities at high loadings are only a fraction of the theoretical (50–75%), it is more realistic to expect practical volumetric energy densities

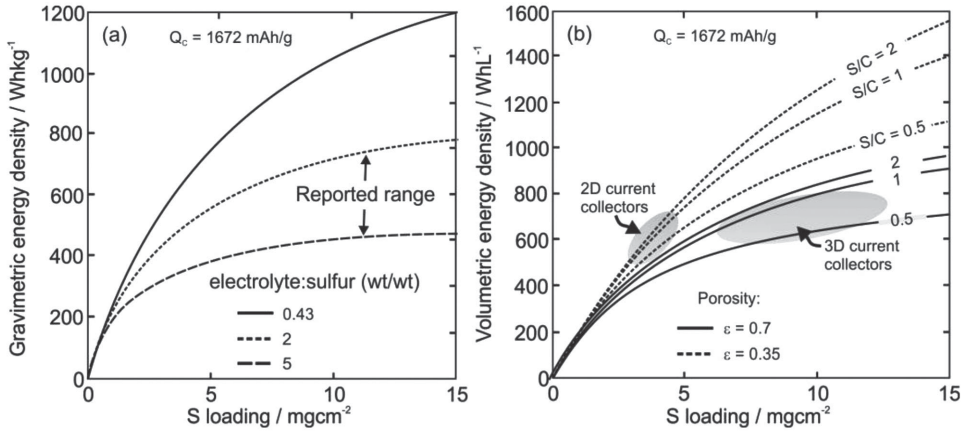

Figure 9. Effect of electrolyte:sulfur ratio, porosity and S/C on the projected energy density. a) Gravimetric energy density (i.e., specific energy) as a function of sulfur loading for various ratios of electrolyte mass to sulfur mass. b) Volumetric energy density as a function of S loading for various porosities and S/C. Each plot assumes that the theoretical capacity of sulfur can be achieved independent of S loading.

of ≈400–500 Wh L^{-1}. For either case, improving the capacity at high loadings while decreasing the electrode porosity as well as decreasing the amount of conductive additive used will be important for improving both the specific energy (gravimetric) and energy density (volumetric).

3.3. All Solid-State Cathodes

All solid-state Li-S batteries have also recently demonstrated significant progress. In this design, a solid Li ion conductor such as Li_xPS_y[90,91] is used to replace the typical ether-based organic electrolyte. The use of solid electrolyte (SE) promises improved safety due to its negligible flammability and also provides a means to effectively inhibit polysulfide dissolution. Japanese researchers Nagata and Chikusa[91] as well as Kinoshita et al.[90] provide sufficient details to discuss their work in the context of our analysis. The former press their all solid mixture to create cathodes with a loading of 4.9 mg S cm^{-2}. The expected negligible polysulfide migration was demonstrated by the high capacity that could be maintained at ≈1600 mAh g^{-1} over 100 cycles for low loading cells operated at a relatively high current density of 1.3 mA cm^{-2}. Despite this exceptional performance, cell assembly required ≈45 mg cm^{-2} of solid electrolyte (SE) as a barrier layer between the anode and cathode leading to projected specific energies of ≈200 Wh kg^{-1} compared to the >600Wh kg^{-1} that could be achieved if a traditional, lightweight, polymer-based separator was used. In addition, these researchers used a Li-In alloy, reducing the cell voltage and the projected energy density by ≈33% compared to the case where pure Li metal is used. The use of a Li-In alloy was presumably used to prevent the reduction of Ge in their $Li_{10}GeP_2S_{12}$ separator layer. Using a similar sulfur loading of 4.3 mg S cm^{-2}, Kinoshita et al.[90] milled sulfur and vapor grown carbon fiber with Li_3PS_4 to prepare their all solid-state cathodes which could achieved 1300 mAh g^{-1} capacity with excellent capacity retention over 50 cycles. This was later shown to be improved by doping their SE with small amounts (1–2 wt%) of room temperature ionic liquids (RTILs).[92] The capacity of these high loading cells remained larger than 1200 mAh g^{-1} for over 100 cycles even at a rate of C/2, which we estimate corresponds to a current density of ≈4 mA cm^{-2}. These researchers used a Si anode for their cell and unfortunately do not report the thickness of their separator layer. In another work, a Li metal anode was used in conjunction with a SE and a low S loading cathode.[27] The SE separator layer was reported to be ≈110 mg cm^{-2}. Trevey et al., prepared cells with a high sulfur loading (2.5–3.5 mg S cm^{-2}) and achieve high capacities; however, they also used 150 mg cm^{-2} of SE as a separator layer.[93] While these thick layers are likely over-estimates to prevent cell shorting, it seems that there is a difficulty in preparing a thin, lightweight SE separator using current materials and approaches. If this challenge is overcome, and their reactivity with Li can be sufficiently addressed, this route appears very promising for future development of safe, stable, high specific energy, Li-S batteries. For example, the performance of the cells prepared by Trevey et al. would exceed 500 Wh kg^{-1} if a conventional separator could be used.

3.4. All-Liquid Cathodes: Catholytes

The concept of using a liquid-phase cathode was first explored in 1979 by Brummer's group after determining that they could achieve high solubility of polysulfides in concentrated solutions of tetrahydrofuran (up to ≈10 M in the form of Li_2S_9).[54,55] This approach has the attractive feature of minimizing the amount of solid, electrically insulating reaction products (i.e., S and Li_2S), which deposit on the electrode and reduce the cell's high rate capabilities. In their study, sulfur solutions of up to ≈5 M (in the form of dissolved Li_2S_x) were used to achieve good capacity retention under the application of relatively high current densities (1–4 mA cm^{-2}). They estimated the ability to engineer batteries with $E \approx 300$ Wh kg^{-1}. This is also commensurate with our predictions as illustrated in **Figure 10**. Without considering any carbon material at the current collector, just the mass of the electrolyte at the highest concentrations, leads to E approaching 300 Wh kg^{-1} (for example, at 6 M sulfur $\rightarrow f_\infty \approx 11$ mg electrolyte per mg sulfur). Only by increasing the effective sulfur concentration can this value be increased.

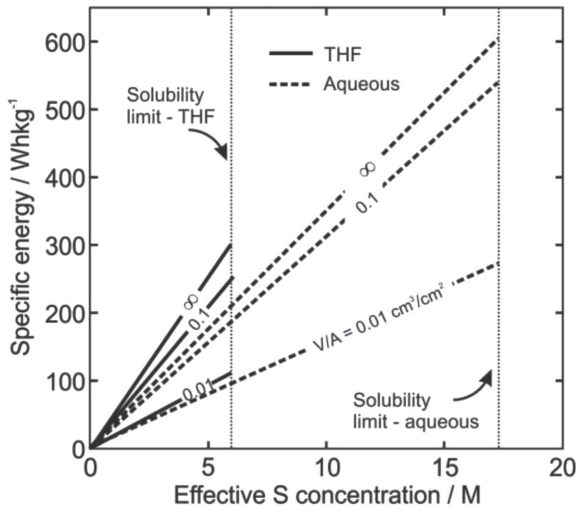

Figure 10. Approximate specific energy of aqueous and non-aqueous catholyte cells as a function of the effective sulfur solution concentration for various ratios of solution volume to separator area (V/A). Calculation assumes the cell voltage is 2.15 V, the full theoretical capacity of sulfur is achievable (1672 mAh g^{-1}) and the density of each catholyte is only 10% larger[94] than the neat solvent alone with the addition of Li_2S_x and other supporting electrolytes. The situation V/A → ∞ gives the highest possible specific energy as the mass of all other cell components is negligible in this limit.

While this and several more recent works have reported on non-aqueous catholyte systems,[36,95,96] PolyPlus Battery Company recently proposed the development of an aqueous catholyte.[97] As lithium is not stable in water, the anode is separated from the aqueous electrolyte by a glassy membrane that selectively transports Li ions but not water. Switching to an aqueous system is motivated by the high solubility of Li_2S in water and its supposed fast dissolution kinetics if solutions beyond the solubility limits are used. According to their patent application, they are able to achieve up to 17.25 M sulfur dissolved in a stoichiometry of Li_2S_4. While this solution was slow to dissolve, Li_2S was found to rapidly dissolve in water at a concentration of only ≈3 M. While promising, several challenges exist with this design. Water was found to decompose at the carbon current collector at potentials near 2 V vs. Li metal. A lead current collector was found to have a higher overpotential (≈1.8 V) but would increase cell weight in practice. Typical Li-S cells discharge to 1–1.5 V vs Li metal for traditional Li-S cells with an average discharge potential of ≈2.15 V. On the other hand, the cell potential was found to be ≈2.3 V in the aqueous electrolyte system which would boost the specific energy by about 7% over the non-aqueous system.

From their design, we estimate that if their maximum concentration of 17.25 M sulfur was used it might be possible to achieve ≈600 Wh kg^{-1} as the ratio of electrolyte volume to current collector area (V/A) approaches infinity. This limit would be approached using a redox flow battery configuration where the electrolyte reservoir is much larger/more massive than the other cell components. This estimate assumes that the density of the aqueous electrolyte at all concentrations is 1.1 g cm^{-3}. The density of an electrolyte has been shown to increase by more than 10% with the addition of 3 M salt.[94] If this trend continues up to 17.25 M, then our estimates in Figure 10 will be off by a factor of ≈1.1/ρ, where ρ is the actual electrolyte density. As discussed in Section 3 above, solid state membranes will be much heavier but this disadvantage could be offset by using a larger catholyte volume since electronic transport through the cathode (catholyte) thickness is no longer a problem as species will, instead, diffuse to and from the current collector. Of course, mixed solid and liquid cathode designs are possible which may be a route to improvements in achievable specific energy as was illustrated by Zhang and Tran discussed above.[36]

4. Cathode Failure Mechanisms

Sulfur-based electrodes undergo a significant change in volume (≈80% increase) as the material converts from S to Li_2S between charged and discharged states.[11,98] The loss of solid material through dissolution of sulfur and polysulfides into the electrolyte likely causes this volume change to be even more drastic.[99] As the lithiation reaction front proceeds from the surface of a sulfur particle to its interior, a considerable tensile stress exists within the particle as the surface layer expands. This differential stress can result in fracture of the sulfur/Li_2S particle unless it is below a critical length scale as has been shown for other materials such as silicon.[100] While this problem can be mitigated by decreasing the size of the sulfur particle or film, the cathode as a whole also undergoes considerable volume change during lithiation/delithiation which can also lead to stress-induced fracture of the cathode network. In order to accommodate the volume change, it has been found that elastomeric binders such as styrene-butadiene-rubber (SBR) work to enhance cycle stability as their high elongation at break (250–700%) and low modulus (2–10 MPa) can reversibly accommodate the volume expansion.[101,102]

Recently, Elazari et al. performed a detailed structural and chemical analysis of sulfur cathodes extracted from Scion's prototype cells after various cycle numbers.[99] Atomic force microscopy was used to illustrate the transition from rough to smooth to granular morphology of sulfur prior to cycling, after 1 cycle and after 25 cycles. After 25 cycles, the electrodes were found to reach an equilibrium and did not significantly change thereafter. The authors also mapped out the electronically conductive domains on the sulfur electrode using conducting probe AFM. In the initial cycles, the relative amount of conductive surface area was high (≈90%) while after 25 cycles, an insulating film developed which reduced the conductive surface area to only ≈7.5%. They also noted the frequent observation of isolated chunks of sulfur that were electrically isolated from the conductive phase of the battery, a situation that would lead to low sulfur utilization. Cracking and large holes/voids in the cathode were also observed. It was suggested that these frequent voids were a result of large sulfur chunks present after initial cathode fabrication which dissolved and redistributed upon cycling leaving behind defects in the cathode. Allegedly such a situation would facilitate cracking as well as the electrical isolation of regions within the cathode. While it may be unimportant to uniformly disperse sulfur in the host matrix to achieve high capacity, as discussed in Section 2, the dispersion

state may in fact have a considerable effect on cycle-life due to these mechanical effects.

By carrying out a systematic analysis of cycled S/FGS composite cathodes, Feng et al.[103] observed an insulating film covering the cycled cathode material. Various spectroscopic techniques were used to determine that this insulating film was composed of insulating species such as Li_2CO_3, Li_2SO_3, Li_2SO_4, and $COSO_2Li$. The formation of these compounds was attributed to a reaction between the residual functional groups on the FGSs with the Li and S during cycling and suggests that the chemistry of the carbonaceous material used may be important in controlling the reversible capacity.

5. Managing Polysulfides for Improved Cycle Life

Another major aspect of cathode design has been to develop strategies which slow or even prevent the transport of polysulfides from the cathode to the anode where they can react to form an insoluble precipitate such as Li_2S. This phenomenon is thought to be the main cause of decreasing cathode capacity and reduced Coulombic efficiency. The various approaches developed to manage these polysulfides are reviewed in the following sections.

5.1. Covalent Attachment

As discussed in Section 3, a promising set of high capacity, high loading battery results have been obtained for sulfur electrodes based on sulfurized polyacrylonitrale (S-PAN). This material is synthesized by heating PAN in the presence of sulfur at a temperature of ≈280–300 °C.[75,82,83] Zhang has recently provided a critical analysis of the structure of this material by comparing literature observations with his own work.[81] It was concluded that S-PAN exists as short $–S_x–$ segments which are covalently bound to the ribbon-like PAN backbone. As illustrated by Raman spectroscopy, the original PAN backbone structure is dehydrogenated, creating sp^2 hybridization of the carbon and yielding a similar structure to polyacetylene.[83] This transformation renders the material electronically conductive. Typically, this method yields a composite containing ≈30–50 wt% covalently bound sulfur after the thermal treatment.[81] Covalent attachment provides chemical stability such that the sulfur-based cathode can even be operated in carbonate-based electrolytes which are known to react irreversibly with free polysulfides and may thus also be suitable as high specific energy cathodes for Li-ion batteries.[75,83] In fact, it was recently demonstrated that an all carbon-based Li-ion system can be assembled from S-PAN cathodes and graphite, an anode that requires the carbonate-based electrolyte for optimal function.[104] However, there are no convenient and scalable methods for pre-lithiating these electrode materials. This remains a challenge that must be addressed in order to replace lower capacity Li-ion battery cathodes. The ability to cycle in carbonate-based electrolytes provides flexibility in terms of anode design, improves safety and enables manufacturers to use an established supply chain as these electrolytes are used in current Li-ion systems. In fact, improvements in cycling were found in carbonate-based electrolytes over ether-based ones as polysulfide solubility is reduced in the former.[105] While sulfur is initially covalently bound in the S-PAN molecular composite, polysulfides can be liberated during the reaction and these can be solubilized in ether-based electrolytes making failure and cycle-life not significantly different compared to more conventional approaches which use cathodes based on elemental sulfur.

5.2. Non-Covalent Interactions

5.2.1. Carbonaceous Host Materials

In addition to providing a high specific surface area conductive support for both S and Li_2S, some carbonaceous materials are also thought to confine polysulfides and slow capacity fade. This kinetic trapping of polysulfides was first discussed by Ji et al. for sulfur infiltrated into an ordered, mesoporous carbon and has since been used to explain improvements in cycle-life for a wide variety of high surface area carbonaceous materials.[11] Most recently, materials based on graphene oxide or reduced graphene oxide have shown promise as sulfur immobilizers.[106,107] Other strategies to retain polysulfides have been to embed sulfur into hollow carbon spheres[86,108,109] or even carbon nanotubes.[110] All of these methods have slowed degradation to varying extents but a substantial decrease in capacity of 20-30% is typically observed over 100–200 cycles.

5.2.2. Polar Host Materials

The interactions between non-polar carbonaceous hosts and polar, ionic polysulfides are weak in nature and likely responsible for their eventual release into the electrolyte.[44,46,48,111] It has been suggested that other polar materials such as oxygen-containing polymers, surfactants, metals or metal oxides might have a higher affinity for polysulfides.[11] The first approaches involved using polyethylene oxide modified carbonaceous materials such as mesoporous carbon[11] or reduced graphene oxide[102,107] to achieve improved capacity retention over controls. In fact, it was shown that reduced graphene oxide containing a large number of residual functional groups was also effective in retaining polysulfides.[107] For example, Ji et al. demonstrated that graphene oxide reduced thermally, at low temperatures, and thus containing a large number of residual functional groups, enabled stable cycling at low rates (0.1C) at capacities near 900 mAh g^{-1} S.[107] Their ab initio calculations indicated that hydroxyl and epoxide functional groups could facilitate strong adsorption of polysulfide species to the functionalized graphene.

Furthermore, high surface area metal oxides have also been used to partially substitute carbonaceous materials as sulfur immobilizers. Various materials such as SiO_2,[36] TiO_2, [44–46] and Al_2O_3[112] have been used for this purpose. In the first example of such a strategy,[111] mesoporous silica (SBA-15) was mixed with a mesoporous carbon which was melt infused with sulfur. The high surface area (≈1100 m^2 g^{-1}) for adsorption by the SBA-15 acted as a polysulfide reservoir to retain polysulfides in the cathode compartment during charge/discharge. This significantly improved

capacity retention over controls without SBA-15. A similar approach but using various phases of TiO_2 was investigated by the same group demonstrating capacities of more than 750 mAh g^{-1} over 200 cycles.[44] Another strategy was demonstrated by Seh et al. who created sulfur-TiO_2 yolk shell nanostructures.[45] A TiO_2 coating was applied to encase sulfur nanoparticles. However, the key was to dissolve some sulfur from the core to account for the volume expansion upon lithiation, which would otherwise crack the TiO_2 shell. Using this principle they demonstrated capacities of nearly 700 mAh g^{-1} after 1000 cycles at 0.5C. Atomic layer deposition of Al_2O_3 has also been investigated, however, cathodes were relatively low in capacity and cycle-life was not as good at the previously discussed TiO_2 cases.[46,112]

5.2.3. Conducting Metal Oxides

In contrast to TiO_2 which is a low conductivity semi-conductor, sub-stoichiometric oxides of titania, referred to as Magnéli phases (Ti_nO_{2n-1}) exhibit much higher electrical conductivities which are similar to graphite.[113] Several very recent studies have illustrated the promise of one of these materials, Ti_4O_7, as a conductive additive capable of inhibiting the polysulfide shuttle effect.[47,48] Tao et al.[47] demonstrated an impressive 99% capacity retention over 100 cycles at 0.1C for sulfur electrodes of moderate loading (1–3 mg composite cm^{-2}) and relatively high sulfur contents (65–75 wt% sulfur). Density functional theory calculations were used to explore the interactions between the Ti_4O_7 and polysulfide species. The low co-ordination of Ti_4O_7 was found to facilitate strong adsorption compared to TiO_2. At nearly the same time, the Nazar group reported[48] on Ti_4O_7-based electrodes and demonstrated similarly impressive capacity retention at higher rates and over longer cycling. (**Figure 11**) A fade rate of only 0.06% per cycle was observed over 500 cycles at 2C. These authors also confirmed the strong interactions between the metal oxide surface and sulfur experimentally via in operando X-ray absorption near edge structure (XANES). Compared to a similar sulfur electrode with a carbonaceous conductive additive, the Ti_4O_7-based electrode's capacity retention was improved by a factor of two.

Titanium disulfide has also been shown effective as a conductive additive due to its high electronic conductivity and potential to strongly bind polysulfides.[49] Seh et al. prepared electrodes from TiS and Li_2S in an effort to prelithiate sulfur for use with alternative anodes.[49] At practical loadings of 5.32 mg Li_2S cm^{-2} (3.7 mg S cm^{-2}) they were able to achieve high areal capacities of 3 mAh cm^{-2}. However, as discussed above, the relatively low capacity and high fraction of conductive additive (TiC + carbon black) lead to projected specific energies of only ≈230 Wh kg^{-1}, which is the highest reported for an electrode based on Li_2S, but far from what is achievable with sulfur-based cathodes. Their lower loading cells (≈1 mg Li_2S cm^{-2}) were capable of retaining over 77% of their initial capacity over 400 cycles at 0.5C.

5.2.4. Metal Organic Frameworks

The mesoporous chromium trimesate metal organic framework (MOF) was first used by Demir-Cakan et al.[50] to demonstrate

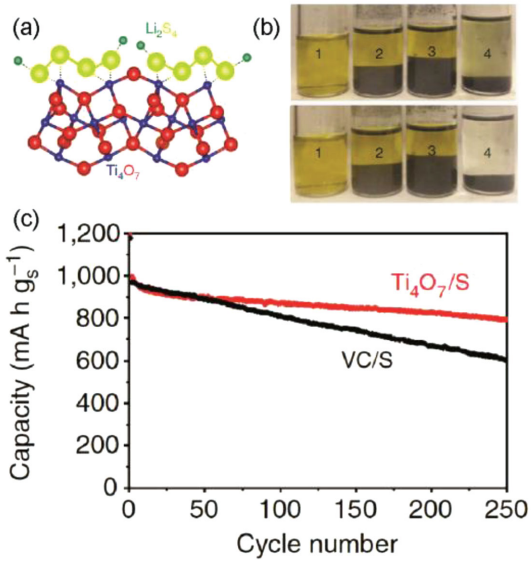

Figure 11. Demonstration of the strong binding interaction of polysulfides with Ti_4O_7. a) A schematic showing the electron density transfer between Li_2S_4 and TiO_X (yellow = S, green = Li, blue = Ti, red = 0). b) Sealed vials of a Li_2S_4/THF solution (1) and after contact with graphite (2), carbon black (3) and Ti_4O_7 (4) immediately (top) and after 1h of stirring (bottom). c) Cycling performance of Ti_4O_7/S-60 and carbon black/S-60 at C/2 for 250 cycles corresponding to a current density of ≈0.75 mA cm^{-2} from the S loading information given. Adapted with permission. [48] Copyright 2014, Macmillan Publishers Ltd,

improved capacity retention over both mesoporous carbon and silica-based materials for sulfur encapsulation.[50] More recently, Zheng et al. demonstrated that nickel-based MOFs could also act as effective scaffolds for sulfur.[51] However, it was only possible to achieve ≈10 wt% of conductive additive in the current system which limited the capacity and rate capabilities of the Ni-MOFs used. Density functional theory calculations were used to illustrate the strong Lewis acid/based interactions between the MOF and various polysulfide intermediates. These interactions lead to enhanced cycle-life, as illustrated by cathodes retaining 89% of their sulfur capacity after 100 cycles at 0.1C.

5.3. Physically Blocking Polysulfide Migration: Core–Shell Structures

Several important strategies involve physically restricting polysulfides from diffusing out of the cathode compartment either by coating sulfur particles with a layer that hinders their movement either sterically or electrostatically. For example, polysulfides are negatively charged and therefore a strategy to prevent their migration away from the cathode is to coat the cathode material with a positively charged polymer such as Nafion.[114] By either using Nafion as a binder in a carbon/sulfur composite cathode [114] or by encasing the cathode completely in a Nafion layer,[115] significant enhancements to cycle-life have been achieved. The general strategy of coating sulfur with a material which blocks polysulfide diffusion is known as a "core–shell" structure. Various other examples of encapsulating sulfur with graphene,[106] conductive polymers such as

polypyrrole[116] or PANI[117] have been described. Moving from an electrically insulating polymer coating (i.e., Nafion) to electronically conducting coatings improve the electronic transport and thus sulfur utilization while aiding in the retention of polysulfides. As already discussed above, the "yolk–shell" TiO_2 coated sulfur cathodes developed by Seh et al.[45] are an example of an advanced core–shell structure that is engineered with some void space between the sulfur and the shell to allow for the volume expansion expected upon the formation of Li_2S.

5.4. Reducing Polysulfide Solubility

There are many different electrolyte systems that have been studied for use in Li-S batteries and these systems were recently reviewed by Scheers et al.[118] Of these various systems, gel polymer electrolytes (GPEs),[119] ionic liquids (ILs),[23] "solvent-in-salt" systems,[120] and all solid-state electrolytes (SEs)[27,90,91] are thought to be promising strategies for either reducing polysulfide solubility or hindering diffusion out of the cathode.

5.4.1. Gel-Polymer Electrolytes

GPEs are polymer networks swollen with a typical, liquid-phase battery electrolyte which have the useful safety feature that the electrolyte resists leakage.[119] While it is argued, based on a phenomenological viewpoint, that polysulfide diffusion in these systems should be hindered, this has not been thoroughly investigated.[118] However, several studies have reported improvements in cycle-life over controls indicating that the GPE is affecting the system in a positive way.[118,121]

5.4.2. Ionic Liquid Electrolytes

While it is often quoted that ILs do not solubilize polysulfides, this is not necessarily the case as was recently shown by Park et al. who systematically analyzed ILs with various cation and anion structures.[23] They found that all ILs display some measurable solubility (at least ≈ 0.5 mM) and in some cases can be even higher than the typical ether-based solvents used (up to 7.7 M solubility was observed). The cation type was fairly unimportant but the solubility depended largely on the electron donicity of the anion, which governs its ability to dissolve the Li^+ moieties existing on the long chain polysulfides. ILs with a TFSA anion displayed the lowest solubility. Pairing with cations which lead to an IL with the lowest viscosity and thus highest Li ion conductivity enabled the highest capacities.

5.4.3. "Solvent-in-Salt" Electrolytes

Impressive performance improvements were recently demonstrates by several groups[26,120,122] who studied the effects of using electrolyte solutions of LiTFSI in extremely high concentrations (up to 7 M). These high concentrations make the mass and volume of the salt larger than the solvent which has led to the name "solvent-in-salt". The solubility of polysulfides is significantly reduced in these systems which is due to the common-ion effect (i.e., the solubility of a salt will be reduced if another salt is already dissolved at high concentration[123]. While improved cycling has been observed in these cases, a major improvement in all reports has been enhanced initial capacity. This was suggested by Li et al. to be related to the enhanced wettability of their nanoporous carbonaceous electrodes in these high salt concentration solutions.[26] While this is a promising strategy, the major challenge with adopting the solvent-in-salt approach is the high cost of LiTFSI which may make the batteries prohibitively expensive. One of the main advantages driving the development of Li-S batteries is the promise of low cost.

5.4.4. Solid-State Electrolytes

The use of all solid-state electrolytes is the only solution capable of avoiding the polysulfide shuttle problem altogether. This is simply due to the fact that even if there were a propensity for polysulfides to dissolve into the solid matrix, this would be an extremely slow process. Trevey et al. used all solid-state cathodes based on S-PAN and were able to demonstrate a capacity drop of less than 1% at low current densities < 0.1 mA cm^{-2}.[93] Nagata and Chikusa[91] were also able to achieve ≈1600 mAh g^{-1} over 100 cycles for cells operated at a relatively high current density of 1.3 mA cm^{-2}. Similar work by Kinoshita et al. demonstrated all solid-state cells which retained 97% of their initial capacity (1230 mAh g^{-1}) over 50 cycles at a current density of 0.1 mA cm^{-2}.[92] These examples demonstrate the promise of moving towards an all solid-state route in terms of cycle-life. However, as discussed earlier, improved rate performance, reduced separator mass and solid electrolytes compatible with Li metal are required to make this technology commercially feasible.

6. Simultaneous Polysulfide Shuttling and Li Degradation

As discussed in the previous sections, using published approaches, we estimate that it is possible to build Li-S batteries with specific energy exceeding 500 Wh kg^{-1} (at least at rates slower than C/10) using optimized sulfur cathodes if cathode porosity and electrolyte volume can be significantly reduced. In addition, several promising routes exist which enable control over polysulfide transport which have enabled significant improvements in cycle-life. Unfortunately, in many of the cycle-life studies discussed above the active material loadings or current densities were not disclosed making it difficult to conclude whether results are applicable to higher loading cells which require charging at high current densities. Hence, a major challenge that remains to be solved lies in achieving good cycle-life at the more practical loadings (3–5 mg cm^{-2}) and current densities (>1 mA cm^{-2}) required to achieve high specific energy and power. Typically, at these current densities the Li metal anode is known to degrade rapidly, a problem that is often overlooked and may be even more important than managing the polysulfide shuttling phenomenon.[124]

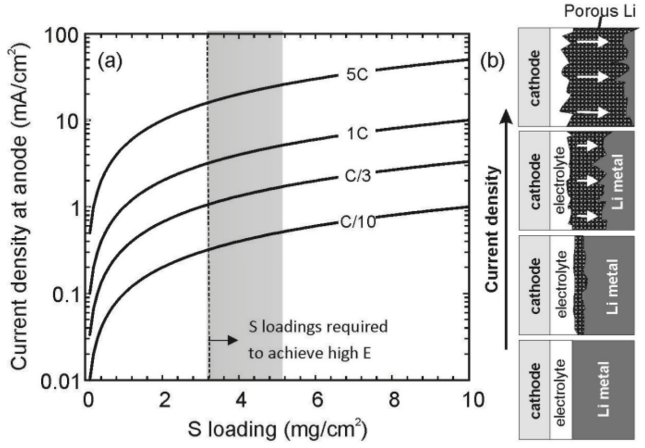

Figure 12. Effect of current density on Li degradation. a) Current density at the Li metal anode as a function of S loading for a variety of charging rates. b) Schematic indicating how the extent of porous lithium formation increases with current density as determined by cross-sectional SEM analysis in Ref.124 Our unpublished results indicate a similar extent of degradation in the ether-based solvents typically used in Li-S batteries.

As shown in **Figure 12**, the morphology of Li metal changes drastically with cycle number especially at the high applied current densities required for battery charging (i.e., Li electroplating).[124] The SEI layer which initially forms on the Li metal anode can form cracks and fissures during the charge/discharge process. This leads to inhomogeneous lithium deposition and reformation of a new SEI layer. The process repeats with each cycle and a porous matrix of Li-SEI develops and grows.[61,62] The continuous deposition of SEI consumes both electrolyte and dissolved polylsulfides and, in theory, can lead to the electrical isolation of pockets of Li metal which have been referred to as "dead" Li.[124] Eventually, it is thought that either the entire electrolyte in the cell dries up[62] or the impedance of the anode becomes so high that the device no longer functions within the set voltage limits.[124] Thus in many cases, the cycle-life depends largely on the amount of excess electrolyte added to the cell.[62] Even without any excess electrolyte, the electrolyte mass dominates all other cell components (see Table 1) and adding electrolyte to compensate would decrease the practical specific energy (see Figure 9a). This is not a practical solution to improving cycle-life.

At small charging current densities (<0.1 mA cm^{-2}) anode degradation is slowed.[124] However, cells with Li metal anodes typically fail after ≈100 cycles at current densities of ≈1 mA cm^{-2} and much more rapidly at higher charging rates.[33] Figure 12 plots current density as a function of cathode loading for several C-rates. A cathode capacity of 1000 mAh g^{-1} sulfur is assumed. For the sulfur loadings which appear to be optimal from our earlier analysis (3–5 mg S cm^{-2}) the current densities required to charge at a slow rate of 10 h exceeds 0.2 mA cm^{-2}. For convenient charging times for electric cars, say 20 min or 5C, this leads to current densities approaching 20 mA cm^{-2}, which would likely lead to cell failure in just a few cycles. To prevent failure, it is critical that strategies be developed to slow or completely prevent the degradation of Li metal. The following paragraphs outline some of the most promising recent strategies.

The use of a dual salt electrolyte to control the growth of the SEI has been demonstrated by Miao et al.[125] using a combination of the FSI- and TFSI- anion in ether-based electrolytes (DOL-DME). They were able to cycle their cells more than 50 times at a current density of 10 mA cm^{-2} and to an extreme depth charge corresponding to 54C cm^{-2} (or 15 mAh cm^{-2}). While their cells did not fail, they observed a porous structure after cycling. However, this structure was supposedly denser and contained less SEI components compared to controls with TFSI- alone.

Ma et al. used a Li_3N layer deposited on Li metal by simply flowing N_2 gas over the side of the Li foil in contact with the membrane separator to protect against degradation when cycling against a thick sulfur cathode.[126] The cathode loading of 2.5–3 mg cm^{-2} was near the optimal range and they were able to demonstrate excellent cycle stability at practically relevant rates of 0.2C and 0.5C. As shown in **Figure 13**, cross-sectional images indicate that the evolution of porous Li metal during cycling was nearly eliminated while the control had a porous SEI layer over 100 µm in thickness. Their cells maintained a capacity of over 700 mAh g^{-1} after 500 cycles which may be the most impressive results we have seen to date for thick sulfur cathodes.

Li metal was coated with 2D atomic crystals such as hexagonal boron nitride (HBN) and graphene by Yan et al. in an attempt to inhibit Li metal degradation.[127] Atomically thin films of these materials were grown on copper metal current collectors by carbon vapor deposition (CVD). Li metal was electrodeposited and found to grow between the HBN/graphene films and the copper substrate, presumably being transported through defects and grain boundaries in the films. These coatings were found to improve the Coulombic efficiency even at high current densities (1–3 mA cm^{-2}) and large depths of charge (5 mAh cm^{-2}). However, the films did not completely inhibit morphological changes of the Li metal during cycling. The thin layers had no measurable effect on the resistance in the system, indicating that the partially blocking layers did not impede Li ion transport to a significant extent. Also, in recent work, Zheng et al.,[128] coated Cu with a carbon film templated on a colloidal crystal of carbon spheres as illustrated in **Figure 14**. After burning out the spheres, Li metal was plated between the carbon layer and the copper substrate in a similar fashion. Again, the films exhibited good Coulombic efficiency with cycling (99% over 150 cycles) at 1 mA cm^{-2}, but a lower depth of charge corresponding to 1 mAh cm^{-2} was used. Other works coated a membrane separator directly using a layer-by-layer approach to fabricate Li ion conducting membranes from graphene oxide/polymer composites.[129] The resulting films cycled for longer than controls without shorting by dendrite growth but cycling was only carried out at a current density of 0.2 mA cm^{-2}. As of yet, no studies have demonstrated a combination of high specific energy, good cycle-life and Coulombic efficiency, despite significant progress in all of these areas independently.

7. Summary and Recommendations

The analysis provided in this review has identified some of the design criteria and materials/cell design strategies that are most

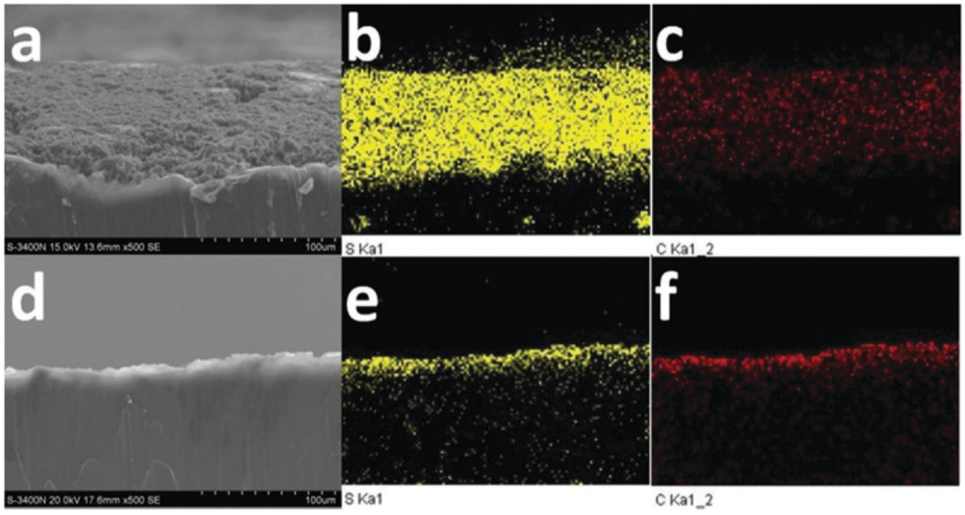

Figure 13. Preventing Li metal degradation with thick, in situ deposited Li_3N layers. a) Cross-sectional SEM image of Li metal control after 100 cycles. b,c) Corresponding energy dispersive X-ray mapping of sulfur (b) and carbon (c). d) Cross-sectional SEM images of Li_3N passivated Li metal after 100 cycles. e,f) Corresponding energy dispersive X-ray mapping of sulfur (e) and carbon (f). Reproduced with permission.[126] Copyright 2014, Royal Society of Chemistry.

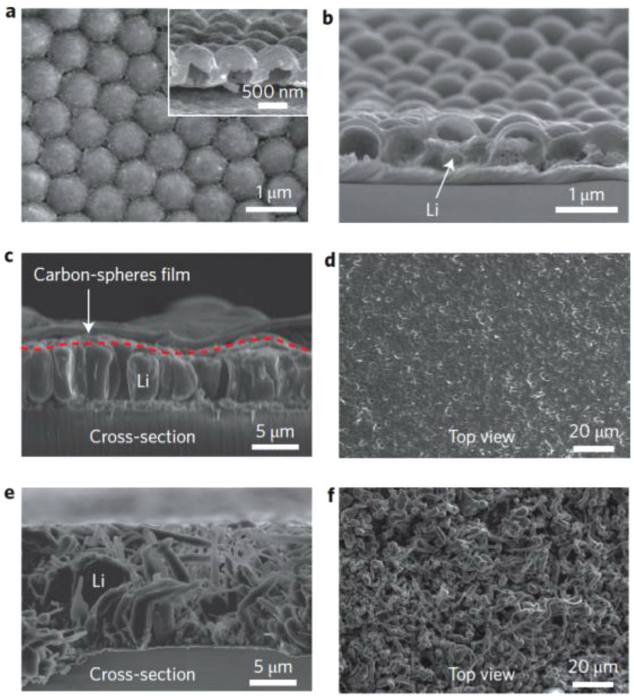

Figure 14. Li metal deposition on a Cu substrate with and without carbon nanosphere modification. a) Top-view SEM image of hollow carbon nanospheres after the initial SEI formation process. Inset: the hollow carbon nanosphere structure is preserved after SEI coating. b) Cross-sectional SEM image showing initial deposition of Li metal under carbon nanospheres. c) Deposited Li metal elevates the hollow carbon nanosphere thin film due to weak binding with the substrate. The carbon nanosphere coating allows more uniform Li ion flux, and the deposited Li metal is columnar rather than dendritic. d) Top-view SEM image showing the smooth surface of the electrode with the carbon nanosphere modification. e) For the electrode without carbon nanosphere modification. f) Corresponding top-view SEM image of the electrode without modification. Reproduced from Ref. [128] with permission from Macmillan Publishers Ltd, copyright 2014.

promising for achieving high specific energy Li-S batteries with improved cycle-life. Since it is often challenging to articulate cathode performance improvements due to large differences in active material loading, sulfur fraction and the resulting cathode capacity, we have introduced a simple correction factor to account for these differences. The results of this comparative analysis have led to the following conclusions and recommendations: 1) When the cathode loading is below ≈2 mg cm^{-2}, the projected specific energy of effectively all literature reports surveyed is below the level expected for advanced Li-ion batteries and thus provides no significant advantage over the current state-of-the-art. For various cathode materials cast onto a 2D Al foil current collector, the optimal loading range was found to be ≈3–5 mg S cm^{-2}. In this range, the use of several conductive additives such as graphene, carbon nanotubes and some conductive polymers enable specific energies approaching 500 Wh kg^{-1} at rates slower than ≈C/10. Both high specific energy and power has, so far, only been achieved by high surface area carbonaceous nanomaterials based on graphene and carbon nanotubes. 2) Various reports using 3D current collectors to increase the active material loading up to ≈13 mg S cm^{-2} have demonstrated significant improvements in capacity density (in mAh cm^{-2}) over current Li-ion technologies. However, our analysis indicates that these improvements do not necessarily lead to an increase in specific energy, due to the excess mass of current collector and conductive additive used. From the estimates presented, these strategies can also achieve $E \approx 500$ Wh kg^{-1} over a range of active material loadings (5–13 mg S cm^{-2}), which is very similar to what can be achieved using conventional 2D current collectors in the optimal loading range discussed in the previous point. As the Li metal degradation rate is linked directly to current density which increases with active material loading, it may prove beneficial to work at the lowest loadings required to achieve high specific energy. Otherwise, the development of porous Li metal and the growth of dendrites are expected to cause rapid cell failure. 3) The few reports that discuss the electrolyte volume/mass

required to cycle their cells indicate that current cathode designs require a significant excess of electrolyte beyond what would be expected if a typical void fraction of 0.35 is assumed. This excess electrolyte decreases the specific energy estimated to below ≈250 Wh kg^{-1}, which is within the range expected to be achievable by Li-ion batteries. Thus a focus on reducing the electrolyte content is required to advance significantly beyond Li-ion technologies. 4) Estimates of the volumetric energy density of the Li-S systems reviewed indicate that they may, at best, match the performance of Li-ion batteries unless cathode architectures with reduced void fraction, reduced conductive additive and increased capacity at high S loadings are devised. 5) All-solid-state Li-S batteries have emerged as the only strategy that is capable of completely eliminating the polysulfide shuttle phenomenon. Several studies have demonstrated impressive cycling results, in some cases being able to achieve over 50 cycles above 1600 mAh g^{-1}. However, the current downfalls of these systems are the apparent difficulty in preparing thin, lightweight, solid electrolyte separator layers. While we project that several studies could achieve 500–600 Wh kg^{-1} with traditional separators, this number drops to ≈200 Wh kg^{-1} for the thick solid electrolyte separators used. Furthermore, few studies use pure Li metal as an anode due to the reactivity of many solid electrolytes, pointing to the importance of designing solid electrolyte chemistries with both improved stability and conductivity. 6) All-liquid catholyte-based Li-S batteries also hold promise for achieving high specific energy. While we project that non-aqueous catholyte systems can achieve a maximum of 300 Wh kg^{-1} (which is already well-above Li-ion), due to their limited solubility, aqueous catholyte systems may be capable of achieving up to 600 Wh kg^{-1}. While promising, the use of Li metal in an aqueous cell will be a technical challenge. Further work in this area is necessary to experimentally validate these claims. 7) A large number of studies aimed towards inhibiting polysulfide transport from the cathode to anode, have been able to demonstrate significant improvements in cycle-life over controls by strengthening the interactions between polysulfides and various conductive host materials. Many of these studies have been carried out on cathodes with low S loadings or for which the S loading is not specified. While studies on more practical S loadings are required, charging at higher current densities will accelerate porous lithium formation and confound any analysis of polysulfide migration effects. 8) The formation of porous Li metal with cycling at rates higher than 0.1 mA cm^{-2} leads to electrolyte depletion and/or an impedance increase due to the formation of "dead" regions within the Li metal. This degradation has been shown to cause rapid capacity fade and eventual cell failure in Li metal cells where cathode degradation or polysulfides are not present. In most studies it is difficult to determine whether failure is due to cathode degradation, polysulfide migration or the formation of porous Li metal. Further work in this area is required to separate out these failure modes, particularly for systems which show promise for achieving high specific energy.

Acknowledgements

This work was partially supported by an Advanced Research Projects Agency – Energy award #DE-AR0000319. The authors would like to thank P. Liu, J. Xiao, J. Liu, and G. Graff for their helpful input. The authors declare financial interests in Vorbeck Materials Corp. that manufactures functionalized graphene under the trade name Vor-x.

Received: January 16, 2015
Revised: February 25, 2015
Published online:

[1] J.-M. Tarascon, M. Armand, *Nature* **2001**, *414*, 359.
[2] V. Etacheri, R. Marom, R. Elazari, G. Salitra, D. Aurbach,. *Energy Environ. Sci.* **2011**, *4*, 3243.
[3] N. S. Choi, Z. Chen, S. A. Freunberger, X. Ji, Y. K. Sun, K. Amine, G. Yushin, L. F. Nazar, J. Cho, P. G. Bruce, *Angew. Chem. Int. Ed.* **2012**, *51*, 9994.
[4] G. Petrecca, *Energy Conversion and Management* Springer, New York **2014**, p. 25.
[5] D. Larcher, J. Tarascon, *Nat. Chem.* **2015**, *7*, 19.
[6] P. G. Bruce, S. A. Freunberger, L. J. Hardwick, J.-M. Tarascon, *Nat. Mater.* **2012**, *11*, 199.
[7] U. DOE, *EV Everywhere Grand Challenge Blueprint*, in US Department of Energy. January **2013**.
[8] *USABC Goals for Advanced Batteries for EVs*, 2006; Available from: http://uscar.org/guest/index.php (accessed March 2015).
[9] R. C. Weast, M. J. Astle, W. H. Beyer, *CRC Handbook of Chemistry and Physics*, Vol. *69*. CRC Press, Boca Raton, FL **1988**.
[10] Scion Power has demonstrated prototype cells with a claimed specific energy of 350 Wh kg^{-1}.
[11] X. Ji, K. T. Lee, L. F. Nazar, *Nat. Mater.* **2009**, *8*, 500.
[12] Y. Zhang, Y. Zhao, A. Konarov, D. Gosselink, H. G. Soboleski, P. Chen, *J. Power Sources* **2013**, *241*, 517.
[13] N. Li, M. Zheng, H. Lu, Z. Hu, C. Shen, X. Chang, G. Ji, J. Cao, Y. Shi, *Chem. Commun.* **2012**, *48*, 4106.
[14] M.-S. Park, J.-S. Yu, K. J. Kim, G. Jeong, J.-H. Kim, Y.-N. Jo, U. Hwang, S. Kang, T. Woo, Y.-J. Kim, *Phys. Chem. Chem. Phys.* **2012**, *14*, 6796.
[15] X. Yang, L. Zhang, F. Zhang, Y. Huang, Y. S. Chen, *ACS Nano* **2014**, *8*, 5208.
[16] M. U. M. Patel, N. D. Luong, J. Seppala, E. Tchernychova, R. Dominko, *J. Power Sources* **2014**, *254*, 55.
[17] W. Bao, Z. Zhang, W. Chen, C. Zhou, Y. Lai, J. Li, *Electrochim. Acta* **2014**, *127*, 342.
[18] J. Xie, J. Yang, X. Y. Zhou, Y. L. Zou, J. J. Tang, S. C. Wang, F. Chen, *J. Power Sources* **2014**, *253*, 55.
[19] C.-S. Kim, A. Guerfi, P. Hovington, J. Trottier, C. Gagnon, F. Barray, A. Vijh, M. Armand, K. Zaghib, *J. Power Sources* **2013**, *241*, 554.
[20] L. N. Wang, H. R. Byon, *J. Power Sources* **2013**, *236*, 207.
[21] Y. Zhao, Y. G. Zhang, Z. Bakenov, P. Chen, *Solid State Ionics* **2013**, *234*, 40.
[22] J. W. Park, K. Yamauchi, E. Takashima, N. Tachikawa, K. Ueno, K. Dokko, M. Watanabe, *J. Phys. Chem. C* **2013**, *117*, 4431.
[23] J.-W. Park, K. Ueno, N. Tachikawa, K. Dokko, M. Watanabe, *J. Phys. Chem. C* **2013**, *117*, 20531.
[24] Z. A. Zhang, W. Z. Bao, H. Lu, M. Jia, K. Y. Xie, Y. Q. Lai, J. Li, *ECS Electrochem. Lett.* **2012**, *1*, A34.
[25] S. S. Zhang, *J. Electrochem. Soc.* **2012**, *159*, A1226.
[26] J. T. Lee, Y. Zhao, S. Thieme, H. Kim, M. Oschatz, L. Borchardt, A. Magasinski, W.-I. Cho, S. Kaskel, G. Yushin, *Adv. Mater.* **2013**, *25*, 4573.
[27] Z. Lin, Z. Liu, N. J. Dudney, C. Liang, *ACS Nano* **2013**, *7*, 2829.
[28] J. Song, T. Xu, M. L. Gordin, P. Zhu, D. Lv, Y. B. Jiang, Y. Chen, Y. Duan, D. Wang, *Adv. Funct. Mater.* **2014**, *24*, 1243.
[29] Y.-S. Su, Y. Fu, A. Manthiram, *Phys. Chem. Chem. Phys.* **2012**, *14*, 14495.

[30] M. M. Rao, X. Y. Song, E. J. Cairns, *J. Power Sources* **2012**, *205*, 474.
[31] Q. Li, Z. Zhang, K. Zhang, J. Fang, Y. Lai, J. Li, *J. Power Sources* **2014**, *256*, 137.
[32] L. Wang, X. M. He, J. J. Li, M. Chen, J. Gao, C. Y. Jiang, *Electrochim. Acta* **2012**, *72*, 114.
[33] M. Hagen, S. Dörfler, P. Fanz, T. Berger, R. Speck, J. Tübke, H. Althues, M. Hoffmann, C. Scherr, S. Kaskel, *J. Power Sources* **2013**, *224*, 260.
[34] K. Fu, Y. Li, M. Dirican, C. Chen, Y. Lu, J. Zhu, Y. Li, L. Cao, P. D. Bradford, X. Zhang, *Chem. Commun.* **2014**, *50*, 10277.
[35] S. Lu, Y. Chen, X. Wu, Z. Wang, Y. Li, *Sci. Rep.* **2014**, *4*, 1.
[36] S. S. Zhang, D. T. Tran, *J. Power Sources* **2012**, *211*, 169.
[37] H. W. Chen, W. L. Dong, J. Ge, C. H. Wang, X. D. Wu, W. Lu, L. W. Chen, *Sci Rep* **2013**, *3*,1.
[38] Y. G. Zhang, Z. Bakenov, Y. Zhao, A. Konarov, N. L. D. The, M. Malik, T. Paron, P. Chen, *J. Power Sources* **2012**, *208*, 1.
[39] G.-C. Li, G.-R. Li, S.-H. Ye, X.-P. Gao, *Adv. Energy Mater.* **2012**, *2*, 1238.
[40] T. N. L. Doan, D. Gosselink, T. K. A. Hoang, P. Chen, *Phys. Chem. Chem. Phys.* **2014**, *16*, 13843.
[41] X.-B. Cheng, H.-J. Peng, J.-Q. Huang, L. Zhu, S.-H. Yang, Y. Liu, H.-W. Zhang, W. Zhu, F. Wei, Q. Zhang, *J. Power Sources* **2014**, *261*, 264.
[42] J. Cheng, Y. Pan, J. Zhu, Z. Li, J. Pan, Z. Ma, *J. Power Sources* **2014**, *257*, 192.
[43] J. X. Zhang, Z. S. Ma, J. J. Cheng, Y. Wang, C. Wu, Y. Pan, C. Lu, *J. Electroanal. Chem.* **2015**, *738*, 184.
[44] S. Evers, T. Yim, L. F. Nazar, *J. Phys. Chem. C* **2012**, *116*, 19653.
[45] Z. W. Seh, W. Li, J. J. Cha, G. Zheng, Y. Yang, M. T. McDowell, P.-C. Hsu, Y. Cui, *Nat. Commun.* **2013**, *4*, 1331.
[46] Z. Liang, G. Zheng, W. Li, Z. W. Seh, H. Yao, K. Yan, D. Kong, Y. Cui, *ACS Nano* **2014**, *8*, 5249.
[47] X. Tao, J. Wang, Z. Ying, Q. Cai, G. Zheng, Y. Gan, H. Huang, Y. Xia, C. Liang, W. Zhang, Y. Cui, *Nano Lett.* **2014**, *14*, 5288.
[48] Q. Pang, D. Kundu, M. Cuisinier, L. F. Nazar, *Nat. Commun.* **2014**, *5*,1.
[49] Z. W. Seh, J. H. Yu, W. Li, P.-C. Hsu, H. Wang, Y. Sun, H. Yao, Q. Zhang, Y. Cui, *Nat. Commun.* **2014**, *5*, 1.
[50] R. Demir-Cakan, M. Morcrette, F. Nouar, C. Davoisne, T. Devic, D. Gonbeau, R. Dominko, C. Serre, G. Férey, J.-M. Tarascon, *J. Am. Chem. Soc.* **2011**, *133*, 16154.
[51] J. Zheng, J. Tian, D. Wu, M. Gu, W. Xu, C. Wang, F. Gao, M. H. Engelhard, J.-G. Zhang, J. Liu, J. Xiao, *Nano Lett.* **2014**, *14*, 2345-.
[52] R. Yazami, P. Touzain, *J. Power Sources* **1983**, *9*, 365.
[53] A. K. Padhi, K. Nanjundaswamy, J. B. d. Goodenough, *J. Electrochem. Soc.* **1997**, *144*, 1188.
[54] R. D. Rauh, K. M. Abraham, G. F. Pearson, J. K. Surprenant, S. B. Brummer, *J. Electrochem. Soc.* **1979**, *126*, 523.
[55] R. Rauh, F. Shuker, J. Marston, S. Brummer, *J. Inorg. Nucl. Chem.* **1977**, *39*, 1761.
[56] S.-E. Cheon, K.-S. Ko, J.-H. Cho, S.-W. Kim, E.-Y. Chin, H.-T. Kim, *J. Electrochem. Soc.* **2003**, *150*, A800.
[57] J. Gao, M. A. Lowe, Y. Kiya, H. D. Abruña, *J. Phys. Chem. C* **2011**, *115*, 25132.
[58] T. Yim, M.-S. Park, J.-S. Yu, K. J. Kim, K. Y. Im, J.-H. Kim, G. Jeong, Y. N. Jo, S.-G. Woo, K. S. Kang, I. Lee, Y.-J. Kim, *Electrochim. Acta* **2013**, *107*, 454.
[59] E. Peled, A. Gorenshtein, M. Segal, Y. Sternberg, *J. Power Sources* **1989**, *26*, 269.
[60] E. Peled, *J. Electrochem. Soc.* **1979**, *126*, 2047.
[61] Z. Li, J. Huang, B. Yann Liaw, V. Metzler, J. Zhang, *J. Power Sources* **2014**, *254*, 168.
[62] C. M. López, J. T. Vaughey, D. W. Dees, *J. Electrochem. Soc.* **2009**, *156*, A726.
[63] D. Lv, Y. Shao, T. Lozano, W. D. Bennett, G. L. Graff, B. Polzin, J. Zhang, M. H. Engelhard, N. T. Saenz, W. A. Henderson, *Adv. Energy Mater.* **2014**.
[64] M. U. M. Patel, N. D. Luong, J. Seppälä, E. Tchernychova, R. Dominko, *J. Power Sources* **2014**, *254*, 55.
[65] J. Song, T. Xu, M. L. Gordin, P. Zhu, D. Lv, Y.-B. Jiang, Y. Chen, Y. Duan, D. Wang, *Adv. Funct. Mater.* **2014**, *24*, 1243.
[66] J. Xie, J. Yang, X. Zhou, Y. Zou, J. Tang, S. Wang, F. Chen, *J. Power Sources* **2014**, *253*, 55.
[67] X. Yang, L. Zhang, F. Zhang, Y. Huang, Y. Chen, *ACS Nano* **2014**, *8*, 5208.
[68] L. Zhu, W. Zhu, X.-B. Cheng, J.-Q. Huang, H.-J. Peng, S.-H. Yang, Q. Zhang, *Carbon* **2014**, *75*, 161.
[69] S. Kinoshita, K. Okuda, N. Machida, M. Naito, T. Sigematsu, *Solid State Ionics* **2014**, *256*, 97.
[70] V. Srinivasan, J. Newman, *J. Electrochem. Soc.* **2004**, *151*, A1530.
[71] T. Marks, S. Trussler, A. Smith, D. Xiong, J. Dahn, *J. Electrochem. Soc.* **2011**, *158*, A51.
[72] I. V. Thorat, D. E. Stephenson, N. A. Zacharias, K. Zaghib, J. N. Harb, D. R. Wheeler, *J. Power Sources* **2009**, *188*, 592.
[73] M. A. Pope, S. Korkut, C. Punckt, I. A. Aksay, *J. Electrochem. Soc.* **2013**, *160*, A1653.
[74] L. Wang, X. He, J. Li, J. Gao, M. Fang, G. Tian, J. Wang, S. Fan, *J. Power Sources* **2013**, *239*, 623.
[75] J. Wang, J. Yang, J. Xie, N. Xu, *Adv. Mater.* **2002**, *14*, 963.
[76] A. Manthiram, Y. Fu, Y.-S. Su, *Acc. Chem. Res.* **2012**, *46*, 1125.
[77] A. Manthiram, Y. Fu, S.-H. Chung, C. Zu, Y.-S. Su, *Chem. Rev.* **2014**, *114*, 11751.
[78] X. Li, Y. Cao, W. Qi, L. V. Saraf, J. Xiao, Z. Nie, J. Mietek, J.-G. Zhang, B. Schwenzer, J. Liu, *J. Mater. Chem.* **2011**, *21*, 16603.
[79] M. A. Pope, A. Hsieh, S. Korkut, C. Punckt, I. A. Aksay, unpublished.
[80] Y. Zhang, Z. Bakenov, Y. Zhao, A. Konarov, T. N. L. Doan, M. Malik, T. Paron, P. Chen, *J. Power Sources* **2012**, *208*, 1.
[81] S. Zhang, *Energies* **2014**, *7*, 4588.
[82] A. Konarov, D. Gosselink, T. N. L. Doan, Y. Zhang, Y. Zhao, P. Chen, *J. Power Sources* **2014**, *259*, 183.
[83] J. Wang, J. Yang, C. Wan, K. Du, J. Xie, N. Xu, *Adv. Funct. Mater.* **2003**, *13*, 487.
[84] J. Cesarano, I. A. Aksay, *J. er. Ceram. Soc.* **1988**, *71*, 1062.
[85] Y. G. Zhang, Z. Bakenov, Y. Zhao, A. Konarov, Q. Wang, P. Chen, *Ionics* **2014**, *20*, 803.
[86] A. D. Roberts, X. Li, H. Zhang, *Chem. Soc. Rev.* **2014**, *43*, 4341.
[87] J. Zheng, D. Lv, M. Gu, C. Wang, J.-G. Zhang, J. Liu, J. Xiao, *J. Electrochem. Soc.* **2013**, *160*, A2288.
[88] S. H. Kang, X. Zhao, J. Manuel, H. J. Ahn, K. W. Kim, K. K. Cho, J. H. Ahn, *Phys. Status Solidi A-Appl. Mater.* **2014**, *211*, 1895.
[89] J. Gao, H. D. Abruña, *J. Phys. Chem. Lett.* **2014**, *5*, 882.
[90] S. Kinoshita, K. Okuda, N. Machida, M. Naito, T. Sigematsu, *Solid State Ionics* **2014**, *256*, 97.
[91] H. Nagata, Y. Chikusa, *J. Power Sources* **2014**, *264*, 206.
[92] S. Kinoshita, K. Okuda, N. Machida, T. Shigematsu, *J. Power Sources* **2014**, *269*, 727.
[93] J. E. Trevey, J. R. Gilsdorf, C. R. Stoldt, S.-H. Lee, P. Liu, *J. Electrochem. Soc.* **2012**, *159*, A1019.
[94] R. C. Dougherty, *J. Phys. Chem. B* **2001**, *105*, 4514.
[95] Y. Yang, G. Zheng, Y. Cui, *Energy Environ. Sci.* **2013**, *6*, 1552.
[96] M. Agostini, D.-J. Lee, B. Scrosati, Y. K. Sun, J. Hassoun, *J. Power Sources* **2014**, *265*, 14.
[97] S. J. Visco, Y. S. Nimon, B. D. Katz, L. C. De Jonghe, N. Goncharenko, V. Loginova, *Aqueous electrolyte lithium sulfur batteries* **2014**, Google Patents.
[98] S. S. Zhang, *J. Power Sources* **2013**, *231*, 153.

[99] R. Elazari, G. Salitra, Y. Talyosef, J. Grinblat, C. Scordilis-Kelley, A. Xiao, J. Affinito, D. Aurbach, *J. Electrochem. Soc.* **2010**, *157*, A1131.
[100] Z. Ma, T. Li, Y. L. Huang, J. Liu, Y. Zhou, D. Xue, *RSC Adv.* **2013**, *3*, 7398.
[101] M. Rao, X. Song, H. Liao, E. J. Cairns, *Electrochim. Acta* **2012**, *65*, 228.
[102] M. K. Song, Y. G. Zhang, E. J. Cairns, *Nano Lett.* **2013**, *13*, 5891.
[103] X. Feng, M.-K. Song, W. C. Stolte, D. Gardenghi, D. Zhang, X. Sun, J. Zhu, E. J. Cairns, J. Guo, *Phys. Chem. Chem. Phys.* **2014**, *16*, 16931.
[104] X. He, J. Ren, L. Wang, W. Pu, C. Wan, C. Jiang, *Ionics* **2009**, *15*, 477.
[105] L. Wang, X. He, J. Li, M. Chen, J. Gao, C. Jiang, *Electrochim. Acta* **2012**, *72*, 114.
[106] H. L. Wang, Y. Yang, Y. Y. Liang, J. Robinson, Y. G. Li, A. Jackson, Y. Cui, H. J. Dai, *Nano Lett.* **2011**, *11*, 2644.
[107] L. W. Ji, M. M. Rao, H. M. Zheng, L. Zhang, Y. C. Li, W. H. Duan, J. H. Guo, E. J. Cairns, Y. G. Zhang, *J. Am. Chem. Soc.* **2011**, *133*, 18522.
[108] N. Jayaprakash, J. Shen, S. S. Moganty, A. Corona, L. A. Archer, *Angew. Chem. Int. Ed.* **2011**, *50*, 5904.
[109] E. Shin, M.-S. Kim, W. Cho, S. Oh, *Nanoscale Res. Lett.* **2013**, *8*, 1.
[110] J. Guo, Y. Xu, C. Wang, *Nano Lett.* **2011**, *11*, 4288.
[111] X. Ji, S. Evers, R. Black, L. F. Nazar, *Nat. Commun.* **2011**, *2*, 325.
[112] H. Kim, J. T. Lee, D.-C. Lee, A. Magasinski, W.-i. Cho, G. Yushin, *Adv. Energy Mater.* **2013**, *3*, 1308.
[113] J. R. Smith, F. C. Walsh, R. L. Clarke, *J. App. Electrochem.* **1998**, *28*, 1021.
[114] Y. Cao, X. Li, I. A. Aksay, J. Lemmon, Z. Nie, Z. Yang, J. Liu, *Phys. Chem. Chem. Phys.* **2011**, *13*, 7660.
[115] H. Schneider, A. Garsuch, A. Panchenko, O. Gronwald, N. Janssen, P. Novák, *J. Power Sources* **2012**, *205*, 420.
[116] Y. Fu, A. Manthiram, *Phys. Chem. Chem. Phys.* **2012**, *116*, 8910.
[117] W. Zhou, Y. Yu, H. Chen, F. J. DiSalvo, H. D. Abruña, *J. Amer. Chem. Soc.* **2013**, *135*, 16736.
[118] J. Scheers, S. Fantini, P. Johansson, *J. Power Sources* **2014**, *255*, 204.
[119] Y. Zhao, Y. Zhang, Z. Bakenov, P. Chen, *Solid State Ionics* **2013**, *234*, 40.
[120] L. Suo, Y.-S. Hu, H. Li, M. Armand, L. Chen, *Nat. Commun.* **2013**, *4*, 1481.
[121] H.-S. Ryu, H.-J. Ahn, K.-W. Kim, J.-H. Ahn, J.-Y. Lee, *J. Power Sources* **2006**, *153*, 360.
[122] E. S. Shin, K. Kim, S. H. Oh, W. I. Cho, *Chem. Commun.* **2013**, *49*, 2004.
[123] H. Le Chatelier, *CR Acad. Sci.* **1894**, *118*, 638.
[124] D. Lv, Y. Shao, T. Lozano, W. D. Bennett, G. L. Graff, B. Polzin, J. Zhang, M. H. Engelhard, N. T. Saenz, W. A. Henderson, *Adv. Energy Mater.* **2014**, *5*, 1400993.
[125] R. Miao, J. Yang, X. Feng, H. Jia, J. Wang, Y. Nuli, *J. Power Sources* **2014**, *271*, 291.
[126] G. Ma, Z. Wen, M. Wu, C. Shen, Q. Wang, J. Jin, X. Wu, *Chem. Commun.* **2014**, *50*, 14209.
[127] K. Yan, H.-W. Lee, T. Gao, G. Zheng, H. Yao, H. Wang, Z. Lu, Y. Zhou, Z. Liang, Z. Liu, *Nano Lett.* **2014**, *14*, 6016.
[128] G. Zheng, S. W. Lee, Z. Liang, H.-W. Lee, K. Yan, H. Yao, H. Wang, W. Li, S. Chu, Y. Cui, *Nat. Nanotechnol.* **2014**, *9*, 618.
[129] S. H. Lee, J. R. Harding, D. S. Liu, J. M. D'Arcy, Y. Shao-Horn, P. T. Hammond, *Chem. Mater.* **2014**, *26*, 2579.